CHANGES WITHIN LAYERED LITHIUM ION BATTERY CATHODE MATERIALS DURING CYCLING DETERMINED BY ^{6,7}Li NMR

By MARK DUNHAM, B. Eng. & Bio. Sci.

A Thesis Submitted to the School of Graduate Studies in Partial Fulfillment of the

Requirements for the Degree Master of Applied Science

McMaster University

McMaster University MASTER OF SCIENCE (2015) Hamilton, Ontario (Chemistry)

TITLE: Changes Within Layered Lithium Ion Battery Cathode Materials During Cycling Determined by ^{6,7}Li NMR

AUTHOR: Mark J. R. Dunham, B. Eng & Bio. Sci. (McMaster University)

NUMBER OF PAGES: 100

CHANGES WITHIN LAYERED LITHIUM ION BATTERY CATHODE MATERIALS DURING CYCLING DETERMINED BY ^{6,7}Li NMR

The increased demand for electric vehicles in recent years has driven the development of Li ion battery technology, yielding interesting trends in cathode materials. The layered cathode material $Li(Ni_{1/3}Mn_{1/3}Co_{1/3})O_2$ gives 30% more reversible lithium extraction than the earlier $LiCoO_2$ and the "overlithiated" material $Li(Li_{0.2}Mn_{0.54}Ni_{0.13}Co_{0.13})O_2$ gives a semi-reversible capacity 25% higher than $Li(Ni_{1/3}Mn_{1/3}Co_{1/3})O_2$.[1,2] ^{6,7}Li MAS NMR and ^{7}Li MATPASS NMR were used to investigate the relation between the lithium ion and metal positions within these materials. It was found that $Li(Ni_{1/3}Mn_{1/3}Co_{1/3})O_2$ showed a preference for Li ions to associate with Co at high voltages, that Mn^{4+} and Ni^{2+} showed some association and that the metals were not highly ordered. $Li(Li_{0.2}Mn_{0.5}Ni_{0.13}Co_{0.13})O_2$ showed a decrease in transition metal layer lithium upon cycling, in agreement with previous models, an ordering of the metal ions with the reinsertion of the lithium ions and a significant change in structure on deep discharge.[3] These results will hopefully lead to more accurate modelling of the materials, understanding of reversibility and to increased reversible capacities in future cathode materials.

Additionally work was done to enable high rate *in-situ* NMR spectra in which spectra are obtained from a cell while cycling in the bore of an NMR spectrometer. A Teflon Swagelok-style cell was designed and the effectiveness of solenoid and saddle coils were tested. It was found that for a 6 mm diameter cathode with a Li metal anode, at least half of the signal intensity could be obtained with a saddle coil whereas the signal was not detected when using a solenoid coil.

Acknowledgements

There are several people whom I want to thank for their help in this project. Firstly, I want to thank Dr. Kris Harris for his assistance in the implementation of the MAT and MATPASS pulse sequences, for his time spent explaining the details of NMR as well as for his knowledge of the details of processing programs without which the analysis of HENMC would not have been feasible.

I want to thank Dr. Gillian Goward for allowing me to join the group despite not being trained as a chemist. Her balance of disciplined expectations, understanding and encouragement made graduate school less painful than it could have been.

I want to thank my labmates whose support, senses of humour, listening and singing skills made it a joy to walk into the office each day.

Most of all, I would like to thank the scientists and physicists of the past whose contributions to human knowledge have enabled the kinds of analysis I have used and the battery technologies which make electrical vehicles feasible. I specifically want to thank Clare Grey and Nicolas Dupre for their cataloging work in the field of solid state NMR; their review paper cited many times acted as a Bible which I constantly referred to over the course of my studies.

Table of Contents

List of Figures

List of Tables

Chapter 1: Introduction

1.1 Motivation

Within recent decades, many studies have measured an increase in atmospheric CO_2 levels which have increased from approximately 280 ppm to 395 ppm since 1750.[1] This, coupled with the fact that oil, natural gas and coal are non-renewable resources which will inevitably be depleted, leads to the conclusion that energy should be used more efficiently, that new sources must be used and these should be developed sooner rather than later. In Canada, 31% of our total energy consumed was used for transportation purposes and this generated 37% of our greenhouse gas emissions.[2] Considering that most of this energy comes from non-renewable resources, this sector represents a significant problem/opportunity for the development and application of new technology.

Electric vehicles are advantageous for multiple reasons. Firstly, electric motors are significantly more efficient than internal combustion engines (Tesla’s drivetrain is approximately 88% efficient, compared to about 35% for the modern internal combustion engine).[3] Additionally, energy can be recovered by regenerative braking in electric vehicles, which is not a feature of conventional vehicles, contributing further efficiency. Arguably the most significant advantage is that renewable, emission-free sources of energy can be used and their cost can be less than the equivalent gasoline for other vehicles.

However, one of the largest hindrances to the adoption of electric vehicles is the current state of energy storage technology. The energy density of secondary cells has been increasing over the last fifty years and the development of secondary (reversible) lithium ion batteries has enabled the use of laptops, electric vehicles and battery powered wheelchairs (Figure 1.1). However, the cost, gravimetric and volumetric energy density, and lifetime of batteries still leave internal combustion powered vehicles as the choice of the majority of the transportation market.[4]

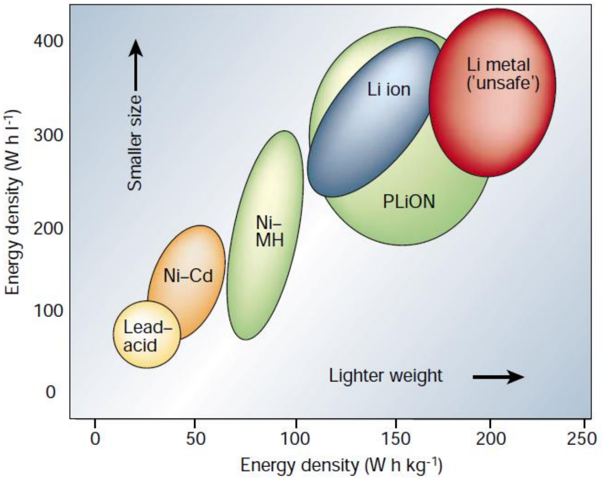

Figure 1.1 The ranges of gravimetric and volumetric energy densities shown by the common kinds of electrochemical cells.[4]

1.2 Aspects of the Functioning of Lithium Ion Batteries

Lithium ion batteries, at their most basic, consist of a cathode which houses oxidized lithium ions and another component (usually a transition metal ion) which can be reversibly oxidized and reduced as lithium ions are extracted and inserted. They also contain an anode where the lithium ions move to, and are reduced, upon charging. The cell also contains an electrolyte which must be capable of dissolving lithium ions and have a high electronic resistance to prevent internal short circuiting.[5] As the main function of the electrolyte is to transport lithium ions, both high ionic conductivity and a minimum intercathode distance are desirable to decrease the internal resistance to ion movement. A diagram of the general lithium ion battery is shown below in Figure 1.2.

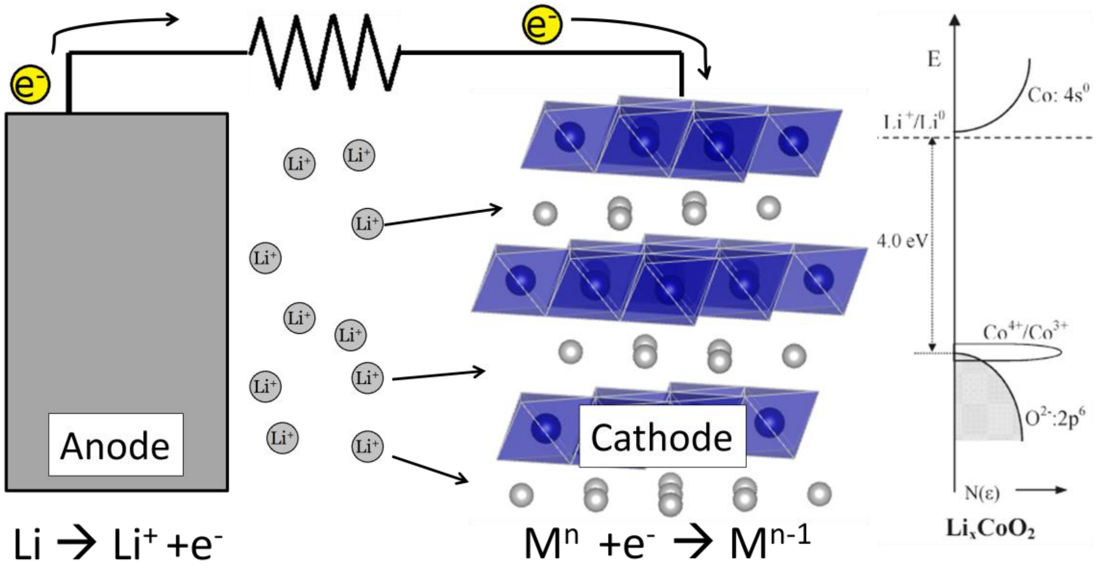

Figure 1.2 The basic functioning of a lithium ion battery during discharge. This would be reversed during charging. The right side shows the bands structure of $LiCoO_2$.[5]

As cell voltages rise to increase energy density within the cell, a concern is the electrolyte stability window; the electrochemical potentials of materials must not be outside that of the HOMO and LUMO of the chosen electrolyte (see Figure 1.3 below).[5] Differing electrolyte types have different windows of stability; polymers and inorganic solids usually have a large window which will generally allow cathodes to be charged in excess of 5V relative to Li/Li^+ without reacting. However, these materials usually have low ionic conductivities and thus can only supply low currents. The electrolyte used for the experiments discussed is 1M $LiPF_6$ in ethylene carbonate (EC)/dimethyl carbonate (DMC), which is not oxidized until ~5V and still has a high ionic conductivity.[5]

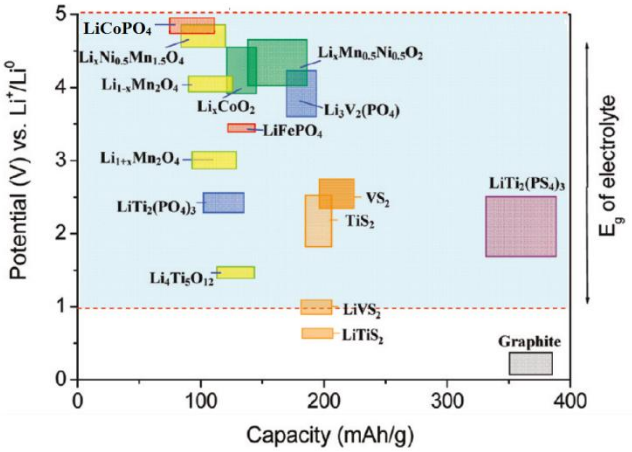

Figure 1.3 A diagram of the electrolyte stability window for EC/DMC and the voltages of cathode materials.[5]

Another concern thought to be a hazard was the oxidation of the oxygen anions. This occurs in materials when they are oxidized to the energy level of the oxygen 2p band. In general, the metal redox centers are at slightly higher energy than this though in some materials, it is possible to create oxygen gas (usually after oxidizing the metal beyond a 3+ oxidation state).[5]

1.3 Methods of Analysis of Cathode Materials

X-ray diffraction is one of the typical methods to analyze solid state materials. It relies upon diffraction of coherent X-rays from a material and their constructive interference at angles dependent on the material's geometry to give information about spaces between the atoms within a material. Combined with other variables such as temperature or voltage, XRD can be used to observe when phase changes occur, whether they are first or second order and how this may change the volume of the material to infer how much stress the cathode experiences. It can also determine the spacing between atoms which can be used to infer the hindrance to Li ion diffusion or changes in the transition metal charge. The magnitude of the diffracted radiation is proportional to Z^2, meaning that it is insensitive to Li.[6] This can be a disadvantage but can be used to determine if Li and a higher atomic number element have exchanged positions. If a slightly larger reflection intensity than expected is obtained from a region of lithium, this means an atom containing more electrons has likely substituted. But, because the metals used in many lithium ion batteries have very similar atomic numbers and numbers of electrons (the range from Mn to Ni is 54-59u), the scattering intensities from these elements are similar. Thus little information about the local ordering of the different metals, which may play a role in a material's stability, can be discerned.

One significant difference between these metals within the typical oxide framework is their oxidation state and their 3d electron configurations. Within the same material, one element may have no unpaired electrons where another may have three. Nuclear magnetic resonance spectroscopy (NMR) can observe a difference in signal depending on which transition metal is present within the material and which oxidation state it occurs in. Furthermore, it is sensitive to lithium, so in these ways it is complementary to X-ray diffraction. NMR can be used to determine, qualitatively or quantitatively, a variety of things about cathode materials. It can be used to determine how much lithium remains in a material over the course of cycling by measuring peak areas, how close two lithium sites are, whether different Li sites exchange with each other, how quickly this exchange occurs, and specifically which lithium sites are withdrawn during the charge.[7] Critically, because the magnetic states of the metal ions influence the lithium chemical shift, in some cases, the location of different metals relative to lithium can be determined.[8]

Scanning Electron Microscopy can be applied to obtain valuable information which supplements that obtained by NMR. Firstly, a simple image of the material can be obtained using SEM which can be used to observe sub-nanometer changes in crystal structure, or more macroscopic changes such as active particle size or carbon contact with the active material. Additionally, electron energy loss spectroscopy can be used to determine the elements in a material as well as their oxidation state. Using this technique, while rasterizing the beam, allows a map of composition and oxidation states to be drawn. This type of characterization is complementary to NMR studies, and is being carried out in the group of Prof. Gianluigi Botton in Materials Science. This data will not be included in the thesis, but combined for joint publication at a later date.

1.4 Layered Cathode Materials

$LiCoO_2$ was the first cathode material used in commercial lithium ion batteries opposite a carbonaceous anode.[9] It is similar to the material used and detailed in thesis in that it is layered where the octahedral sites of a close packed lattice of oxide anions are occupied in alternating layers by lithium ions and the corresponding cations. The structure of $LiCoO_2$ is cubic close packed; three repeating layers of O^{2-}, with Li^+ and Co^{3+} in every other layer between (parameters a = 2.816 A and c = 14.08 A) with space group R3-m known as the α-$NaFeO_2$ structure.[10] This layered structure results in a 2 dimensional plane through which lithium can diffuse. Additionally, it is possible that an observed widening of the oxide layer upon extraction of the lithium ions widens their diffusion pathways decreasing resistance to diffusion.[10] Ion positions are relatively stable upon lithium ion extraction because the crystal field stabilization energy is large for low spin $Co^{3+/4+}$ and thus migration of Co ions to the octahedral sites in the lithium layer, via the tetrahedral sites, has a high energy barrier.[10] However, because of a hexagonal to monoclinic phase transition at 50% extraction, and oxidation of the oxygen 2p band, the capacity is limited to approximately 140 mAh/g.[11] Additionally, a first order phase transition in the region $0.75 < x < 0.93$, in which the unit cell volume changes by approximately 1%, strains the material during charging.[10]

One of the related materials, in that it is also a cubic close packed octahedrally occupied layered material, which has been developed in an attempt to improve cathode performance is $Li(Ni_{1/3}Mn_{1/3}Co_{1/3})O_2$. It was first reported by Naoaki Yabuuchi and Tsutomu Ohzuku in 2003 as having a reversible capacity of 200 mAh/g and being able to be charged reversibly to a higher voltage than $LiCoO_2$ and thus having a significantly higher energy density.[12]

1.5 $Li(Ni_{1/3}Mn_{1/3}Co_{1/3})O_2$

NMC is generally synthesized by one of two methods; the mixed hydroxide method or the sol-gel method. In the mixed hydroxide method, dissolved metal nitrate salts are precipitated as metal hydroxides as LiOH is added. The precipitate is mixed with the stoichiometric amount of the LiOH hydrate and heated until the close packed oxide framework is created. There are several parameters in this process that can be modified such as whether nitrates or sulfates are used, the pH of the solution for precipitation, the heating temperature, cooling rate and atmosphere.[13] The sol-gel method consists of mixing the metal and lithium acetates with citric acid in distilled water and heating to create a viscous gel. This is then dried at ~150°C in a vacuum oven to yield a dry powder which is then calcined at about 450°C and then at 900°C to create crystalline NMC.[14]

It was shown that the X-ray diffraction pattern of NMC was nearly identical to $LiCoO_2$ indicating that it has a similar layered structure; the R3m space group with a = 2.8562 A and c = 14.2045 A (a cell volume of 100.6 A^3, larger than the 96.8 A^3 $LiCoO_2$). Additionally, the XRD showed that upon charging, there was effectively no change in the overall unit cell volume of $Li_x(Ni_{1/3}Mn_{1/3}Co_{1/3})O_2$ (until x = 0.33) compared to a change of 3% in $LiCoO_2$ suggesting that the material would be subjected to less mechanical stress on cycling and retain its capacity better than $LiCoO_2$.[12]

One issue, however, is that Ni^{2+} (r = 0.69 A) has a similar ionic radius to Li^+ (r = 0.76 A) and thus can exchange places with lithium during synthesis. The amount of Ni found in the lithium layer can vary at least from 1% to 6% of Li^+ sites occupied by Ni^{2+} depending on the synthesis method.[13, 15] This is detrimental to the performance by impeding lithium ion motion, and thus increasing the internal resistance of the cell, as well as potentially overall capacity by disallowing the extraction of lithium in the transition metal layer.

One significant difference between $LiCoO_2$ and NMC is that the active redox metal in NMC is Ni rather than Co, which goes from a formal oxidation state of 2+ to 4+ over the course of charging in NMC. This was predicted in Density Functional Theory (DFT) calculations by Ceder et al. They also determined the oxidation states of the transition metals to be Mn^{4+}, Co^{3+} and Ni^{2+} in the pristine material by XANES by comparison to materials of known oxidation state. Also predicted, were that Ni e_g orbitals form a band and that Ni^{3+} does not undergo a disproportionation; all Ni atoms in the bulk maintain a similar oxidation state throughout the course of charging.

As previously stated, little change of the unit cell parameters is seen until at least 65% lithium extraction unlike Li_xCoO_2 which experiences a phase change at $x = 0.5$ limiting the amount of Li which can be reversibly extracted.[10] Charging beyond this point may cause stress on the material and the capacity obtained would probably diminish faster than if the capacity is limited to the region without phase changes.

When a number of compounds of the formula $Li(Ni_yCo_{1-2y}Mn_y)O_2$ were tested for capacity retention, they equalled the performance of $LiCoO_2$ when charged to 4.4V and bettered it when charged to 4.6 or 4.8V. Manthiram et al. showed that $Li_x(Ni_{1/3}Mn_{1/3}Co_{1/3})O_2$ had good capacity retention when charged to 4.6V but that this severely declines when charged to 4.7V. This agrees with Ohzuku's prediction that charging beyond $x = 0.33$, which occurs at approximately 4.6V, would result in strain in the material and subsequent capacity loss.[16] They also investigated the reasons for the apparent stability of the $Li(Ni_{1/3}Mn_{1/3}Co_{1/3})O_2$ phase beyond that of $LiCoO_2$ by analysing the lithium content and oxygen content as the material was chemically oxidized by NO_2BF_4. They found that beyond 65% lithium extraction, the material lost oxygen. This is likely due to the fact that the $Co^{3+/4+}$ orbital lies at the top of the O 2p band as it does in

$LiCoO_2$. They also saw a decrease in the c parameter of the unit cell indicating a change in the arrangement of the oxygen anions.[16]

It was shown that adding cobalt reduces the fraction of Ni that moves to the lithium layer which is expected to contribute to the resistance of lithium ion motion.[17] Understandably then, the increase in cobalt content also results in an increase in rate capabilities.[18]

The effects of the magnetic state of the transition metal can be seen by directly observing the electrons through Electron Paramagnetic Resonance or by observing their effect on nearby nuclei via NMR. Transition metals can contribute a different chemical shift to nearby Li atoms that depends on the angle and number of metal-lithium bonds as well as their electronic configuration. Thus knowing the electronic/magnetic properties of the material is critical for this kind of analysis. It has been determined by many groups that in layered oxide materials Co^{3+} is diamagnetic ($t_{2g}^6\ e_g^0$) whereas, in a pristine state, neither Ni^{2+} ($t_{2g}^6\ e_g^2$) nor Mn^{4+} ($t_{2g}^3\ e_g^0$) are affected by a high spin or low spin designation.[13, 19] In DFT calculations, Ceder et al. asserted that Mn and Ni are anti-ferromagnetic in certain ranges throughout the charge.[14] The magnitude of this interaction was not mentioned though it has been reported that NMC displays paramagnetic behaviour at temperatures above 150°K. Therefore, this coupling would likely not need to be considered in NMR analysis at room temperature.[20]

NMR analysis of NMC has been done by Cahill et al. for the primary purpose of understanding the factors impacting the movement of Ni ions into the lithium layer. Deconvolution of the lineshape and use of information about chemical shift mechanisms and charge balancing within the material allowed a tentative assignment of 3 sites within the material. These pertain to the 3 closest metals in the metal layer directly above and below a given lithium atom (the first coordination sphere). These are shown below in Table 1.1.[13]

Table 1.1. Shift assignment for lithium in the transition metal layers.[13]

Case	Ni^{2+}	Mn^{4+}	Co^{3+}	Frequency
a	1	1	4	Lowest
b	2	2	2	Middle
c	3	3	0	Highest

Zeng et al. also analyzed a number of compounds of the formula $Li(Ni_xMn_xCo_{1-2x})O_2$ $(0.33<x<0)$ by ^6Li MAS NMR and used a statistical analysis to determine that there is preferential association of Ni^{2+} and Mn^{4+} in the pristine material. However, they also found that this is not strictly the case and there are cases where the first coordination sphere is not charged balanced.[21]

While much is known about the material, little work has been done to determine the local structure of the material during charge which is the aim of this study. The aforementioned studies give a wealth of information from which to base interpretation of any future results.

1.6 Overlithiated Cathode Materials

In an attempt to increase the capacity (and thus the energy density) of cathodes, which lags behind that of anode materials, materials known as over-lithiated materials or high energy cathodes were created. These contain excess lithium which in most cases is in octahedral sites within a transition-metal layer (in a structure analogous to regular NMC).

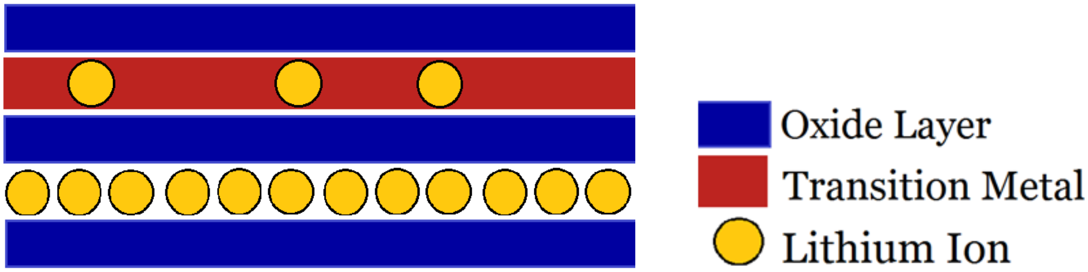

Figure 1.4 The layered structure of HENMC with the excess Li ions occupying sites in the transition metal layer.

By observing charge curves in electrochemical cycles, it can be seen that these materials exhibit a large first charge capacity, which can be in excess of 300 mAh/g, and consists of a rise in voltage until about 4.4V followed by a large plateau region. On subsequent discharges, the capacity is significantly smaller (on the order of 230 mAh/g) though is repeatable on charge and discharge (see Figure 1.5 below). This is in contrast to the 140 mAh/g provided by $LiCoO_2$.

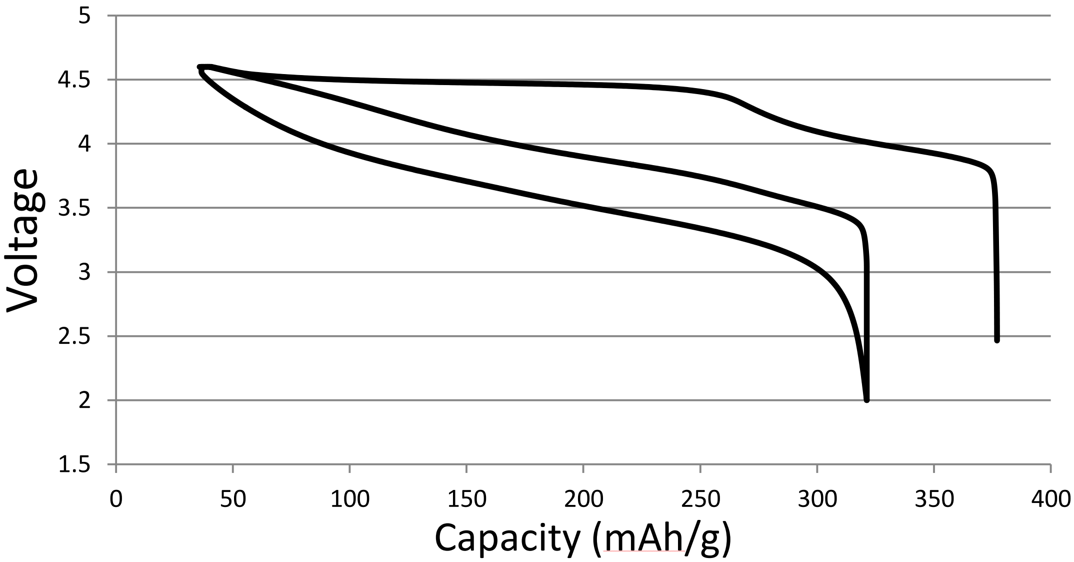

Figure 1.5 The charge curve for the over-lithiated material $Li(Li_{0.2}Mn_{0.54}Ni_{0.13}Co_{0.13})O_2$.

Because of their high capacities and unusual charging characteristics, there are several questions that surround these materials. For instance, the capacity calculated from the oxidation of the transition metals to a 4+ oxidation state does not account for all of the initial or reversible capacity, so where does the excess initial capacity come from? Also of interest is why the first discharge and subsequent charges do not exhibit the same C-V characteristics as the initial charge. If the material does change after the first charge to account for these C-V characteristics, what is the new structure?

Dahn et al. investigated the series of materials $Li(Ni_xLi_{(1/3-2x/3)}Mn_{(2/3-x/3)})O_2$ by *in-situ* XRD and electrochemical cycling measurements. They suggested that the initial voltage rise was due to the oxidation of Ni^{2+} to Ni^{4+} and that the following plateau between 4.5V and 4.7V likely corresponds to the removal of Li_2O from the structure (oxidation of oxygen and withdrawal of a lithium ion to balance the charge). The removal of oxygen from the structure likely meant the movement of transition metals to the lithium layer. They supported these claims by calculating the capacities of the initial voltage rise and a plateau (whose capacity was assumed to be the remaining lithium in the lithium layers) which matched their data well. Based upon inferences from changes, or lack thereof, in the unit cell structure, they claimed that during the plateau region, the transition metals do not change their oxidation state but oxygen is removed. An analysis of the differential capacity of the material (dQ/dV vs V) lead to the conclusion that a segment of the discharge curve is due to the reduction of Mn to a 3+ state.[22] This has been supported by EXAFS data from a stoichiometry very close to the material of interest.[23]

In a study by Manthiram et al., Ti, which occurs as a 4+ ion with no remaining 3d electrons, was substituted for Mn in a series of these high energy materials containing Co and Ni as well. When cycled, the presence of Ti increased the bond strength with oxygen, decreased the amount of oxygen released and significantly reduced the discharge capacities. The conclusion of this study was that the discharge capacity was dependent upon the oxygen loss.[24] This would support Dahn's conclusion that the further reduction of the metals is necessary for the high discharge capacities.

In an effort to explain how parts of the main oxygen framework are lost and yet the unit cell maintains regular, undistorted dimensions, Delmas et al. proposed the "densification model" whereby the structure is compacted (shown below).

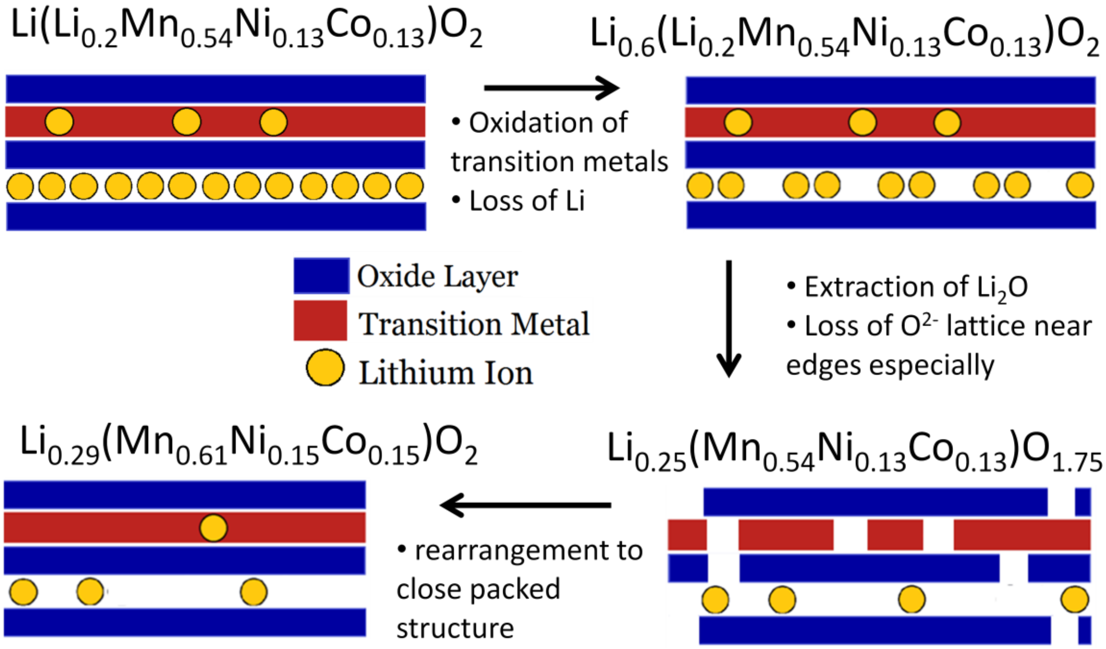

Figure 1.6 Densification model proposed by Delmas et al.[25] The stoichiometries shown are based upon an in-lab cycled HENMC cell.

After charging to ~4.5V and oxidizing the transition metals to 4+ states, the oxygen 2p band is oxidized. This results in the release of oxygen gas leading to the loss of a close-packed structure (see Figure 1.2). This would be less thermodynamically stable than a structure in which all of the ions were close together. In order for the material to become close-packed, migration of both oxide ions, transition metal ions and lithium atoms must happen. Because only Li and O were lost, the stoichiometry of the material changes and the transition metal layer should lose positions for Li.[25]

Another question, as in non-excess materials, is whether any ordering of the transition metal layer exists. Complete order of the transition metal layer has been observed in materials such as Li_2MnO_3 which may be due to a Coulombic driving force for local charge balancing.[26] In analyzing $Li(Ni_xLi_{(1/3-2x/3)}Mn_{(2/3-x/3)})O_2$ by first principles simulations, significant order was seen up to 1000 K. Analysis of the ^{6}Li MAS NMR spectra also showed that peaks assigned to 6 Mn^{4+} neighbours were seen in materials for which this was statistically unlikely. This means that the transition metal distribution was non-random suggesting charge balancing.[27]

Elaborating on the previous studies which had supposed that only Li layer lithium atoms were extracted, Grey and Ceder conducted a combined NMR and computational investigation into which Li atoms are extracted in $Li(Li_{1/9}Mn_{5/9}Ni_{1/3})O_2$. By using approximately known shift contributions from surrounding metals, they determined that there were two transition metal layer lithium sites in the pristine material; those surrounded by 6 Mn^{4+} and those by 5 Mn^{4+} with 1 Ni^{2+}. By NMR, they found that the Li in the transition metal layers were extracted and replaced during cycling resulting in disorder and reordering of the transition metal layer ions. However, after multiple cycles, they saw a decrease in the amount of transition metal layer Li and less defined peaks. They attributed this to transition metal diffusion within their layer so that the lithium which was reinserted was near a range of different metals and may not be reinserted due to the sites not being as favourable as the initial site near 6 Mn^{4+}. Additionally, through calculation, they suggested a necessity for three nearby Li layer vacancies for a Li ion to move downward from the transition metal layer. Likewise, this would cause impedance during cycling by denying lithium layer lithium access to neighbouring octahedral sites while the transition metal layer lithium atom is in a tetrahedral site due to Coulombic repulsion.[28]

While similar materials have been investigated by NMR over the course of cycling, none have shown at which potentials the Li are extracted and returned which would provide valuable insight into how easily they are removed and returned. Additionally, the material which is the target of this study, $Li(Li_{0.2}Mn_{0.54}Ni_{0.13}Co_{0.13})O_2$, contains Co which has been shown to provide benefits in the case of NMC. Thus, knowing how this material specifically functions is of significant interest.[18]

1.7 NMR Overview

Many nuclei, due to their arrangement of protons and neutrons, have a nuclear spin. The reason it is called a spin is that when the nucleus is exposed to a magnetic field, the nuclear magnetic moment will rotate meaning that, in the sense of classical physics, it is a spinning bar magnet with a net angular momentum vector. The nuclear magnetic moment (μ_i) is related to this spin (I_i) by the gyromagnetic ratio (γ) which is a constant specific to each nucleus.

$$\mu_i = \gamma I_i \qquad [1]$$

Because the nucleus has a net angular momentum due to the spin, a magnetic field will create a force on the spin and cause it to rotate about a vector parallel to the field. This rotation is called precession and its frequency (ω_0) depends upon the gyromagnetic ratio according to

$$\omega_0 = \gamma B_0 \qquad [2]$$

where B_0 is the magnetic field strength. Additionally, because the nucleus has a net magnetic moment, the application of a magnetic field results in a splitting of the energies of the nuclear eigenstates; those aligned with the field being of lower energy than those against. The population of these levels, and thus the net magnetic moment of the sample, depend, on the Boltzmann distribution and thus the applied field. That is, a larger field will increase the net magnetic moment of the sample (nearly linearly in the case of NMR) as well as the precession frequency, increasing the flux through the coil and therefore the signal acquired.

Of concern however, are the T_1 and T_2 values for a given nucleus. T_1 describes the exponential rate at which perturbed nuclear spins return to an equilibrium state (aligned with the magnetic field). This is of importance because it determines the speed at which data can be acquired; the nuclei must relax to generate a strong magnetic moment, a subsequent voltage and thus signal during acquisition. The T_2 value describes the rate at which coherence is lost in the transverse plane in which the nuclei precess. The phase of nuclei with the same frequency will be disturbed by transient magnetic fields which can arise from nearby unpaired electrons or moving atoms. If the generated magnetic fields have a frequency component close to the resonant frequency of the nucleus, they can exert torque on the nucleus, moving it and causing a spreading of the magnetization and thus a loss of signal. T_2 relaxation can also occur if atoms move to a site and have a new resonance frequency (chemical exchange). When this occurs during the acquisition of signal its phase will have effectively been changed and consequently the pattern will broaden. The Fourier transform of a single frequency with a very short T_2 can result in a broad peak.

1.8 Nuclei of Interest

Within our materials of interest there are several NMR active nuclei. However, the NMR active nuclei of oxygen, cobalt, manganese and nickel suffer from either low natural abundance or a large quadrupole moment. Li nuclei, however, have been used to investigate the structure of many cathode materials. Li ions are the most mobile species within both electrodes and thus provide an interesting way to investigate changes in the cathodes over the course of cycling. Its shift range in diamagnetic environments is often not more than 10 ppm.[8]

Table 1.2 Variables of interest for the utilized nuclei.[29]

	Natural Abundance (%)	Spin	Gyromagnetic Ratio (rad s^{-1} T^{-1})	Quadrupole Moment (C m^2)
6 Li	7.5	1	0.8220473	-0.00083
7 Li	92.5	3/2	3.2564268	-0.0406

1.9 Chemical Shift Mechanisms

There are several factors which can affect the chemical shift of a nucleus. When a compound is placed in a magnetic field, the electrons will generate a current to oppose this field (to shield the nucleus and reduce the net magnetic field there). Because the electron distribution around a nucleus depends upon the chemical environment, the amount of shielding can vary. This is usually in the range of 0 ± 5 ppm for Li in diamagnetic materials. Additionally, this shielding is anisotropic and so different chemical shifts are obtained for different molecular orientations. In a liquid sample, small molecules tumble quickly so that the shielding is an average for the nucleus and one chemical shift value is observed. In solids, this averaging does not happen in a static sample but this will be discussed in later paragraphs.

A shift mechanism common in metals, called the Knight shift, occurs due to the contribution of lithium s orbitals to crystal orbitals near enough the Fermi level that they contain some unpaired electrons. These electrons will have a net spin, $\langle S_z \rangle$, due to the applied magnetic field and thus contribute a chemical shift.[8] This occurs in lithium metal where the 2s/2p band is occupied and a shift of 200-400 ppm is observed.[30]

If unpaired electrons are present in the material much larger chemical shifts can occur.[8] Electrons have a much higher magnetic moment than nuclei and thus their effect is much larger than that typically seen in coupling to another nucleus. In addition to contributing large anisotropic ranges (due to having their own strong field), electrons can contribute isotropic shifts if they have a finite probability of existing at the nucleus of the element of interest.

The delocalization mechanism is the name given to the “Fermi-contact” orbital overlap which results in unpaired electron density at the nucleus of interest.[8] This can happen directly if the orbital containing the unpaired electron overlaps the nucleus or indirectly by coupling to the electrons in an intervening orbital (often the oxygen 2p orbital (or 2π* band) in an oxide cathode material).[8] This is generally considered to be additive so that multiple surrounding transition metals can contribute a certain amount to the electron spin density at the lithium nucleus. This has been shown by Delmas et al. and Grey et al. and is accepted as a method of analysis within the field. The magnitude and sign of the shift contributed depends upon which orbitals contain the unpaired electrons, the electronic average spin, the number of polarized orbitals between the paramagnetic centre and the Li 2s orbital and their angle of overlap (Figure 1.7). For instance, the shift contributed from a Li-O-Mn^{4+} contact varies from 250 ppm for a 90° to -60 ppm for a 180° contact.[21, 31] The shifts contributed by different atoms and arrangements present in NMC are given below.

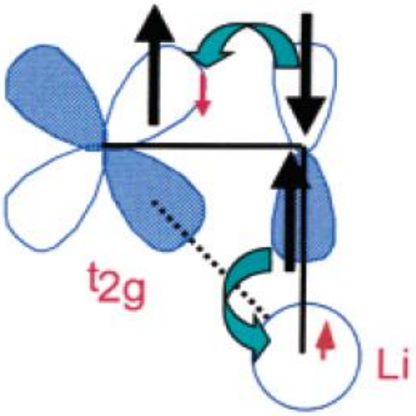

Figure 1.7 Contribution of spin density from a singly occupied t_{2g} orbital to a Li nucleus by indirect 90° Fermi-contact through an oxygen 2p orbital.[8]

Table 1.3 Li chemical shifts obtained from paramagnetic doping listed by the metal-oxygen-lithium angle.[21, 31]

^{6}Li Chemical Shift [ppm]

	Mn^{4+}	Ni^{2+}	Ni^{3+}
90°	250	-30	-15
180°	-60	170	110

^{7}Li Chemical Shift [ppm]

	Mn^{4+}	Ni^{2+}	Ni^{3+}
90°	250	-30	-13
180°	-52	120	112

The polarization mechanism is a separate mechanism by which the alignment of electrons with or against the magnetic field (or exchange coupling with nearby electrons) changes the energy of their atomic orbitals causing different contributions to the crystal (molecular) orbital bands if the overlap is significant. If this shift results in a different electronic contribution to a band with the Li 2s orbital, then there will be spin density at the Li nucleus resulting in a chemical shift. The direction of the shift depends on which spin-orbital is moved to the level of the lithium s band.[8]

While the aforementioned shift mechanisms depend on the electron's probability of being at the nucleus, the magnitude of the through space coupling of a nucleus with an electron's magnetic moment is determined by the term

$$H_{en} = \frac{\mu_0 \mu_e \mu_n (3\cos^2\theta - 1)}{4\pi r^3} \qquad [3]$$

where μ_n is the nuclear magnetic moment which is a constant given by γI_n and μ_e is the averaged electronic magnetic moment.[8] The latter depends upon the applied magnetic field and temperature according to the Boltzmann distribution and is given as

$$\mu_e = g^2 \mu_B^2 S(S+1)B_o/3kT \qquad [4]$$

The average lifetime of a given electronic state, called T_{1e}, can vary covering a range from 10^{-12}s to 10^{-7}. Often, this is fast on an NMR timescale and does not broaden the resonance significantly. Short T_{1e}s are seen in cases where $S > ½$ but broad resonances have been seen in cases involving ions with single spins such as Ni^{3+} (see Figure 1.8 below).[8, 32]

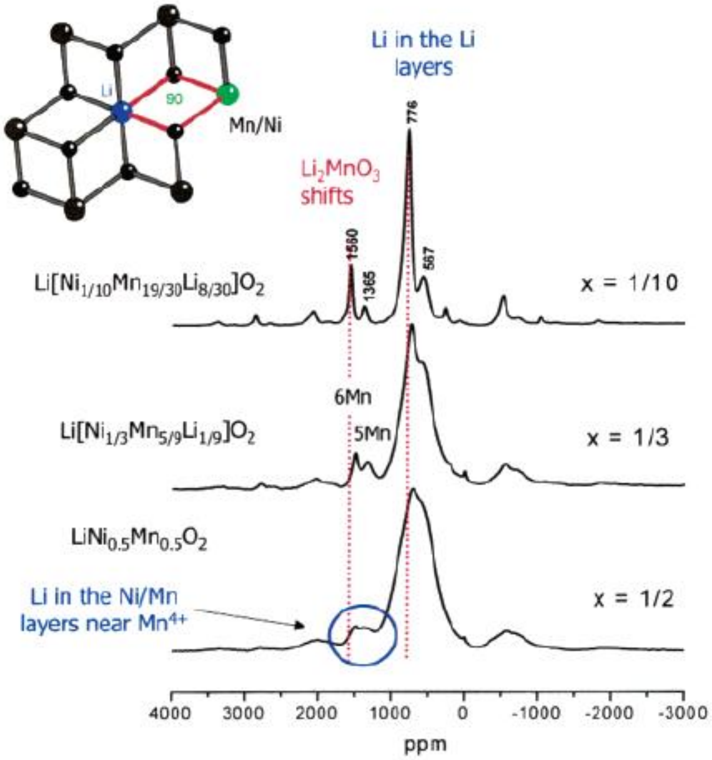

Figure 1.8 Increasing linewidth with the addition of Ni into the structure.[27]

1.10 Overcoming Anisotropy

In solid state NMR, dipolar coupling is another significant concern. This describes the energy of the interaction of the nucleus with the dipolar magnetic field of another nucleus (or an unpaired electron) through space and is given by

$$\hat{H} = -\left(\frac{\mu_0}{4\pi}\right)\gamma_I\gamma_S\hbar\left(\frac{I\cdot S}{r^3} - 3\,\frac{(I\cdot r)(S\cdot r)}{r^5}\right) \qquad [5]$$

Where S and I are the orientation vectors of the magnetic dipoles, and r is a vector pointing from one to the other.[33] Because the energy of this interaction depends on the orientation of the spins (and thus the external magnetic field B_0) relative to the vector between them, the energy of this interaction is also dependent on the sample's orientation relative to the field.[33] With many particles with different orientations, this results in broad patterns which can overlap and hinder clear interpretation of the spectrum. These depend upon the angle to the magnetic field according to $3\cos^2\theta - 1$ which when spun has the average value $\frac{1}{2}(3cos^2\theta_R - 1)(3cos^2\beta - 1)$ where θ_R is the angle between the applied field and the spinning axis and β is the angle between the shielding tensor's z axis and the spinning axis. Though β cannot be easily changed, θ_R can be set to a value of 54.74° so that the term $3\cos^2 \theta_R - 1 = 0$; the shielding anisotropy is averaged and the dipolar coupling becomes 0. The technique of spinning about this angle is called Magic Angle Spinning (MAS).

However, if the speed at which the sample is spun is slow compared to the magnitude of the anisotropy (both values can be measured in Hz), then a series of "spinning sidebands" appear in the spectrum. These are peaks which appear at fixed distances apart from the isotropic peak which are equal to the spinning speed of the rotor (in Hz). If the isotropic pattern is broad, it is possible that the spinning sidebands may overlap and confuse the pattern leading to difficult interpretation. Thus, higher spinning speeds are desirable to prevent overlap and the available spinning frequency can limit the B_0 field used. Likewise, at lower fields, the same spinning speed will cover more ppm and can spread peaks further apart in ppm to resolve the spectrum.

Taking these effects into account will allow us to select the field, spinning speed and techniques to obtain signals from the sample which are then readily interpreted and provide the most information. The work of others in determining the magnitude of each effect in similar materials will also be invaluable in the analysis of the obtained spectra.

Chapter 2: Studies of $Li(Ni_{1/3}Mn_{1/3}Co_{1/3})O_2$

The characteristics of $Li(Ni_{1/3}Mn_{1/3}Co_{1/3})O_2$ have been studied by many methods; electrochemical cycling methods, EIS, XRD, XANES, AAS, EPR and modelling by DFT. It has been established that the structure of the material is the same layered alternating structure as $LiCoO_2$; that the cation oxidation states in the pristine material are Mn^{4+}, Co^{3+} and Ni^{2+}; and that while no long range ordering of the transition metals exist, there is a general association of Mn^{4+} and Ni^{2+} due to coulombic attraction.[34,14,26,35,36] Upon charging, it has been determined that at least 65% of Li can be extracted before oxygen is oxidized, that the unit cell doesn't change volume significantly until about 70% Li extraction and that the main charge compensation for Li extraction in the reversible section is $Ni^{2+} \rightarrow Ni^{4+}$ oxidation. [16, 34, 36] And while nuclear magnetic resonance spectroscopy has been used on the pristine material and derivatives thereof, it has not yet been used to investigate changes during cycling.[13]

The main aim of this study is to elucidate some of what occurs upon cycling; how ordered the metals in the material are, whether Li preferentially occupies any specific sites and how the material's lithium is depopulated. This may give some insight as to why this material does not undergo a phase change at the same level of Li extraction as $LiCoO_2$ and which properties should be sought in future cathode materials. This will also be contrasted with the performance of $Li(Li_{0.2}Mn_{0.54}Ni_{0.13}Co_{0.13})O_2$ in the next chapter.

2.1 Methods

To obtain more information about changes on cycling, electrochemical cells were made. $Li(Ni_{1/3}Mn_{1/3}Co_{1/3})O_2$ material was obtained from the Toda company. Cathode slurries, consisting of an 8:1:1 mixture by mass of NMC : acetylene carbon black : 3 wt% polyvinylidene fluoride dissolved in n-methyl 2-pyrrolidone, were cast on aluminum foil sheets and were heated to 120°C under vacuum to remove the solvent. ½ ” diameter disks of the cathode material were punched and assembled in 2032 coin cells with a 25 μm thick polypropylene separator from Celgard, lithium metal as the anode. These were then charged at a rate of C/20 (the cell’s full capacity based upon lithium content in 20 hours). Each cell was charged at this rate galvanostatically to the desired voltage and then charged potentiostatically until the current was below a C/100 rate. This ensured the cells were within 10 mV of the desired open circuit voltage.

The cathodes were then extracted from the cells, washed with a solution of propylene carbonate to remove electrolyte salts and dried in a vacuum before being packed in an NMR rotor, all within an argon filled glovebox with water content below 0.1 ppm and 5 ppm oxygen.

For all ^{6}Li spectra, the samples were packed into a 1.8 mm NMR rotor and spun to 31.5 kHz in a 4.7T field. A 3.75 μs 90 degree pulse was used before a 2 rotor period Hahn echo with a 35 μs delay after the 180° pulse before acquiring the free induction decay (127 μs after the original 90 degree pulse), so that ringing from the original pulse would not add noise to the signal. The Hahn echo must be rotor synchronized so that the 180 degree (second) pulse occurs an integer number of rotor periods after the 90 degree (first) pulse.

Because of spinning speed limitations, the time before acquisition also has a minimum. The relaxation delay was 0.5s. Because of various time constraints and a low signal to noise ratio, the number of scans acquired differed for the samples.

2.2 ^{6}Li MAS NMR

Nuclear magnetic resonance was the primary technique chosen to investigate the cathode materials. Typically available NMR probes have a maximum spinning speed under 45 kHz; 40 kHz was the maximum speed available for these first experiments. Because the samples could not be spun fast enough to resolve the isotropic peaks in an 11.7T field or 7.05T field, a lower field strength of 4.7T (200 MHz proton) was chosen so that the spinning frequency would allow further separation of the spinning sidebands.

The acquisition of the ^{6}Li signal from the pristine material, while being spun at 40 kHz, resulted in the following spectrum that matched the results of Cahill et al. (Figure 2.1) The main set of peaks between 0 and 1000 ppm correspond to Li in the lithium layer while the small signals at ~1300 ppm correspond to those Li in the transition metal layer.[13]

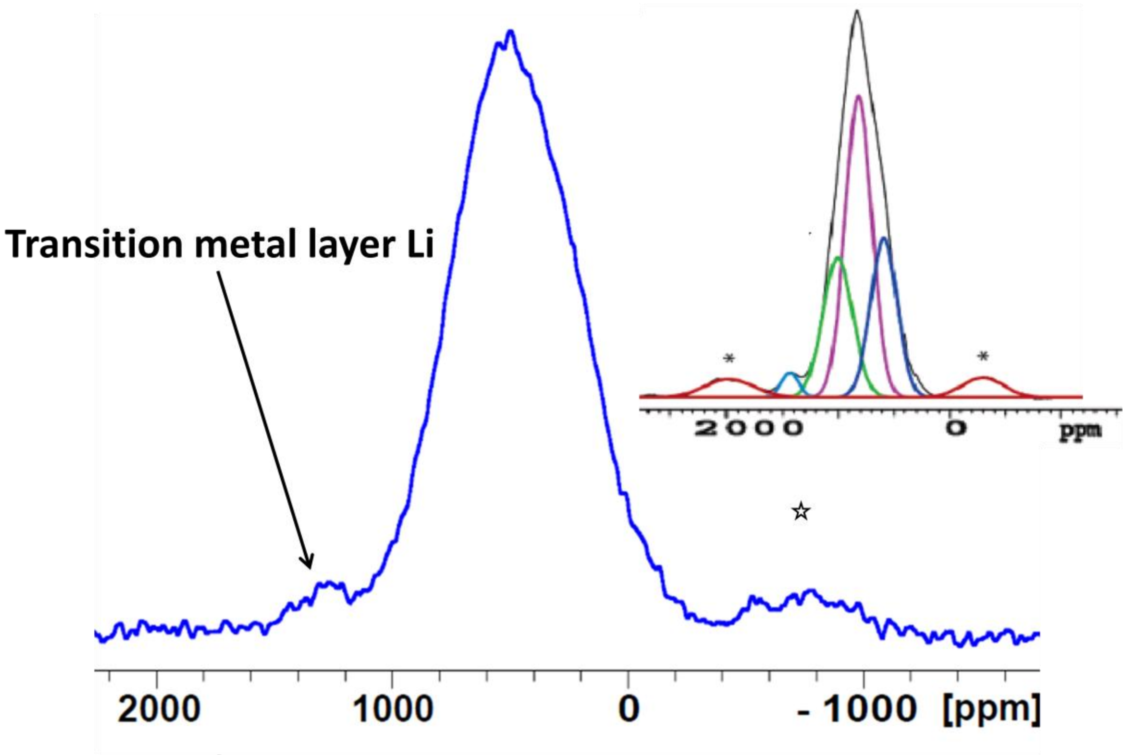

Figure 2.1 40 kHz ^{6}Li MAS NMR of Toda Li(Ni$_{1/3}$Mn$_{1/3}$Co$_{1/3}$)O$_2$ in a 4.7T field. The star denotes spinning sidebands. The figure in the upper right is the deconvolution by Cahill et al.[13]

To determine the effects upon charging, it is critical to know what contributes the chemical shift experienced by each Li ion. As previously stated, the shift contributions for each of the ions present in the range 0.33 > x > 1 for this material were found for ^{6}Li by Grey et al. and for ^{7}Li by Samoson et al. This was done by the addition of small amounts of paramagnetic Ni^{2+} and Mn^{4+} in diamagnetic LiCoO$_2$ and are given below in Table 2.1.[31] These depend on the arrangement of atoms around the lithium (the angle of the metal-oxygen-lithium contact) which are shown in Figure 2.2 for an octahedrally sited lithium ion surrounded by other ions also in octahedral sites.

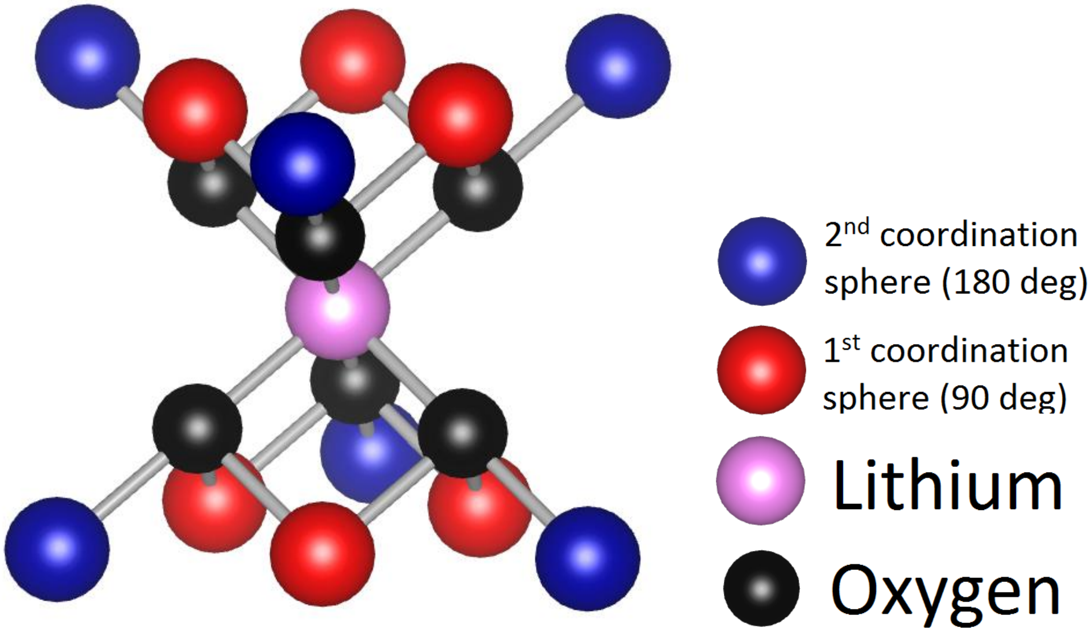

Figure 2.2 The locations of atoms in the first and second coordination spheres relative to lithium.

Table 2.1 Li chemical shifts obtained from paramagnetic doping.[31,21]

^{6}Li Shift [ppm]

	Mn^{4+}	Ni^{2+}	Ni^{3+}
90°	250	-30	-15
180°	-60	170	110

^{7}Li Chemical Shift [ppm]

d	Mn^{4+}	Ni^{2+}	Ni^{3+}
90°	250	-30	-13
180°	-52	120	112

In the following discussion, we attempt to correlate the changing lineshape and chemical shift position of the lithium resonance to the oxidation state changes expected as lithium is removed from the structure. In compensation for the lithium ion extraction, the transition metal ions will be oxidized. The possible changes in the electron configuration may result in changing the electron configurations from paramagnetic (contributing large positive chemical shifts) to diamagnetic (contributing no substantial chemical shift). From the trends in lineshape, we infer the corresponding lithium ion extraction, and oxidation state changes, for both the first and second coordination spheres, based on the cumulative shifts tabulated above.

Upon charging the cells at a C/20 rate, C-V curves such as the one displayed below are obtained. Each marker indicates a potential (relative to Li/Li^+) to which the cell was charged. The variable x is an indicator of Li content in the material considering the formula $Li_x(Ni_{1/3}Mn_{1/3}Co_{1/3})O_2$.

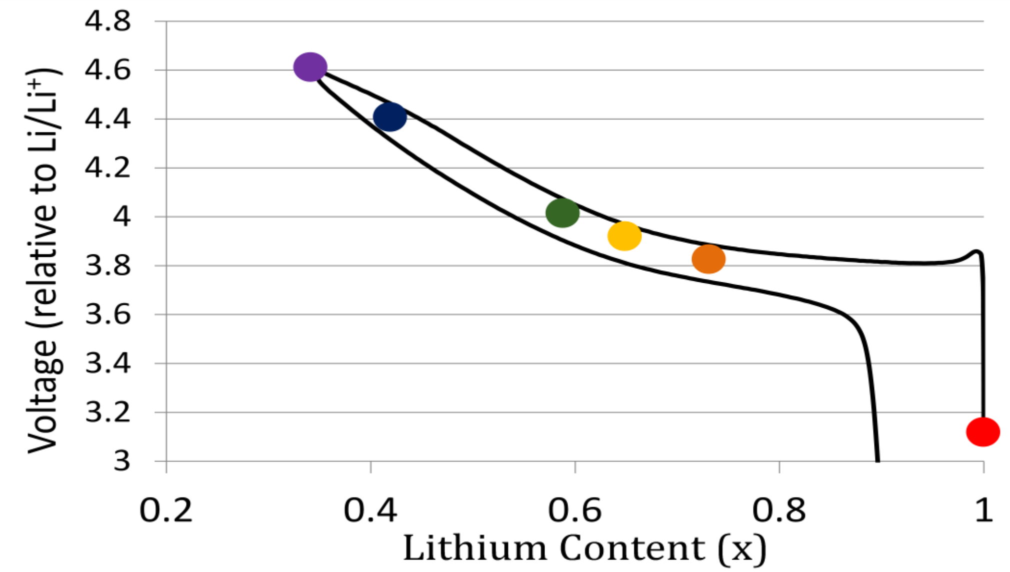

Figure 2.3 Capacity-voltage curve of $Li_x(Ni_{1/3}Mn_{1/3}Co_{1/3})O_2$ on the first charge at a rate of C/20. Each point corresponds to an individual sample and a spectrum in Figure 2.4 below. The points lay between the two curves because potentiostatic charging brings the cathodes to equilibrium at each voltage.

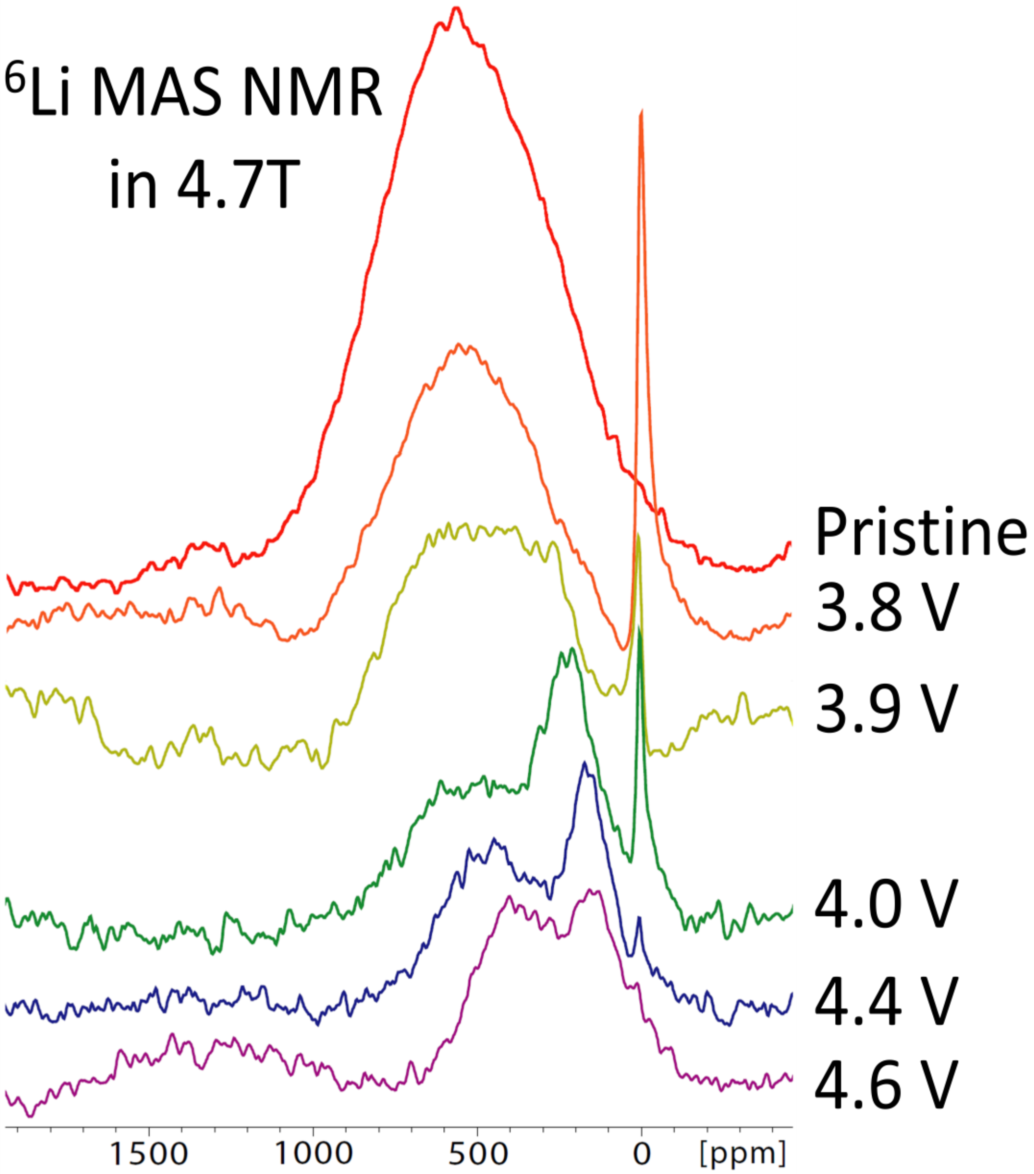

Figure 2.4 Array of ^{6}Li MAS NMR spectra of NMC charged to different voltages (galvanostatically and then potentiostatically) spun at 31.5 kHz in a 4.7T field.

The narrow peak at 0 ppm, corresponding to lithium in a diamagnetic region, is attributed to residual electrolyte salt on the surface. Looking at the lowest frequency peak's chemical shift over the course of oxidation (shown in more detail in Figure 2.5 below), we observed a gradual shift to lower frequency rather than a new peak forming as electrons are removed from Ni. This would suggest that the Ni near the lithium ions change their oxidation state quickly relative to the NMR timescale which would mean high electronic conductivity. This conclusion is in agreement with simulations by Ceder et al. who predicted the existence of a band formed by the Ni e_g orbitals, and with Scrosati et al. who observed an electrical insulator to conductor transition near the beginning of charge.[14, 37]

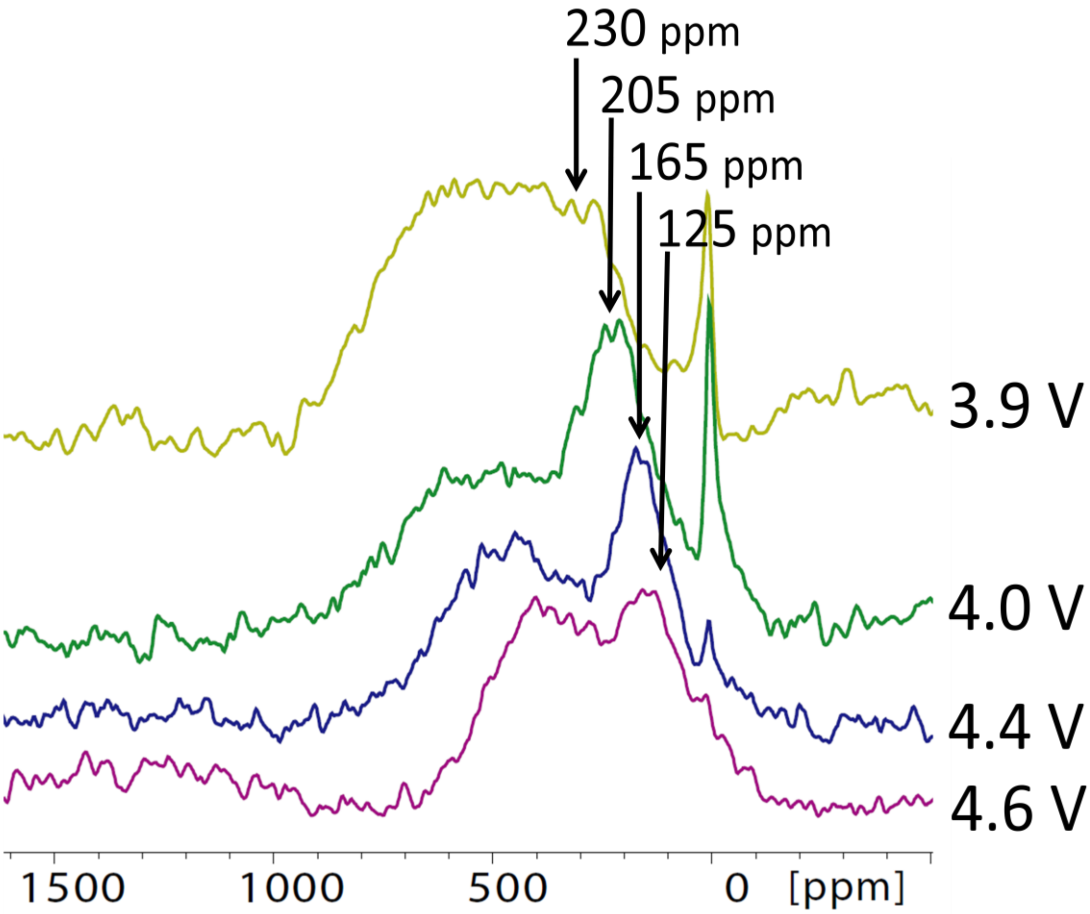

Figure 2.5 Array of ^{6}Li MAS NMR spectra of NMC charged to different voltages. $Ni^{3+} \rightarrow Ni^{4+}$ is expected over the 4.0V to 4.6V range. These spectra are the same as those in Figure 2.4 above.

For the majority of the spectra, the Ni is still in a paramagnetic state (electronic configuration shown below in Figure 2.6) and contributes a large positive shift if it is present in the second coordination sphere of the Li ions. This makes it difficult or impossible to say whether a shift to lower field is due to lithium removal from sites with Mn^{4+} in the first coordination sphere or oxidation of Ni in the second. However, at 4.6V, we can expect that nearly all of the Ni has been oxidized to a diamagnetic state ($t_{2g}^6\ e_g^0$) due to the amount of Li extraction and thus charge compensation which has been shown to come from Ni oxidation (Figure 2.6 below). This would mean that the only Fermi contact shift contribution should be from Mn^{4+}, which allows deciphering the difference in the effect in this spectrum.[36]

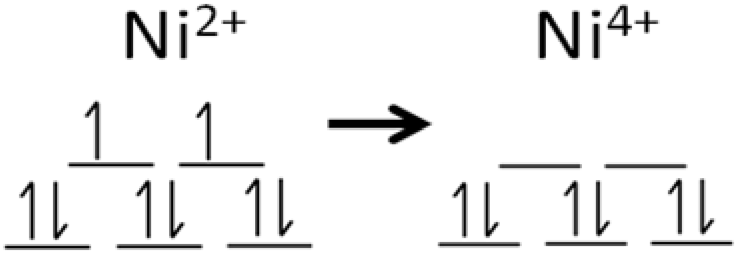

Figure 2.6 The expected distribution of electrons in Ni^{2+} and its oxidation to LS diamagnetic Ni^{4+}.

Considering the shift contributions solely from Mn^{4+} from Table 2.1 means any shift to higher frequency should be due to Mn^{4+} in the first coordination sphere (contributing 250 ppm per Mn^{4+}). Shifts below this would be due to Mn in the second coordination sphere. The lack of signal above 500 ppm suggests that no lithium ions are in sites with 3 Mn^{4+} in the first coordination sphere. However, the signal at and below 500 and 250 ppm means that Li atoms do occupy sites with 1 and 2 Mn^{4+} in the first sphere.

If some Li ions occupy sites with only 1 Mn^{4+} in the first coordination sphere, then to maintain the 1:1:1 stoichiometry of the material (which requires an average of 2 Mn^{4+} in the first sphere), there must also be Li ion sites in the structure with 3 Mn^{4+} in the first sphere. The lack of signal intensity at, and just below, 750 ppm indicates that the lithium has been removed from these sites on oxidation to 4.6V.

The low natural abundance of ^{6}Li coupled with the necessarily low field meant that the signal to noise ratio of the obtained spectra was low. However, it was possible to apply some techniques to improve the signal to noise and perhaps infer more about the material.

2.3 ^{7}Li MAT NMR

To obtain better resolution, ^{7}Li 5π MAT was used.[38] This is a 2-dimensional technique which allows the separation of spinning sidebands which would normally overlap the spectrum if direct ^{7}Li acquisition was used. This consists of a sequence of π pulses, the timing of which varies over the course of the second dimension of acquisition.[38] When Fourier transformed, this results in 2D spectra like the one shown below. The intensity from the spinning sidebands can then be summed to see the spectrum as if acquired at infinite spinning speed.

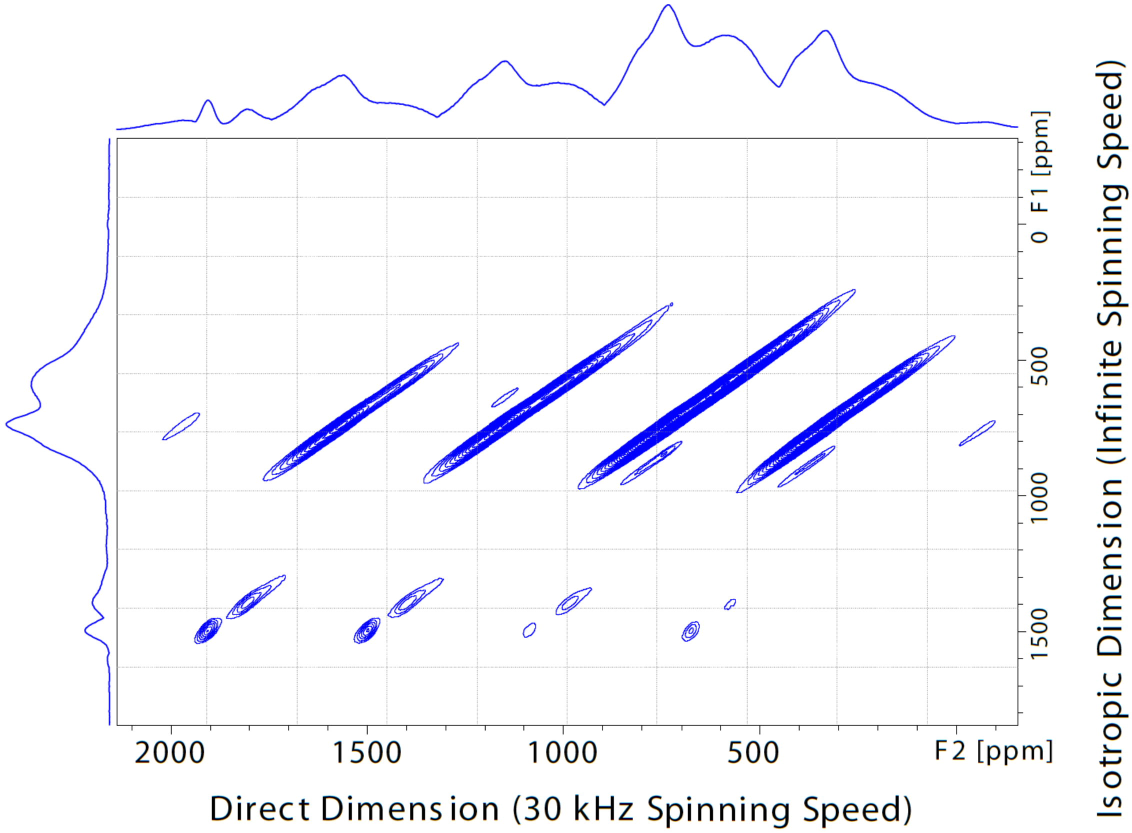

Figure 2.7 The 2 dimensional output of the Fourier transformed MAT acquisition.

The ability to use ^{7}Li, which has a larger magnetic dipole moment and is 12 times more naturally abundant than the ^{6}Li isotope, significantly improves the signal to noise ratio (Figure 2.8). It should be noted that to avoid truncation ripples in the spectra, line broadening is applied in the indirect dimension so the electrolyte peak (at 0 ppm) appears significantly wider than it normally would be.

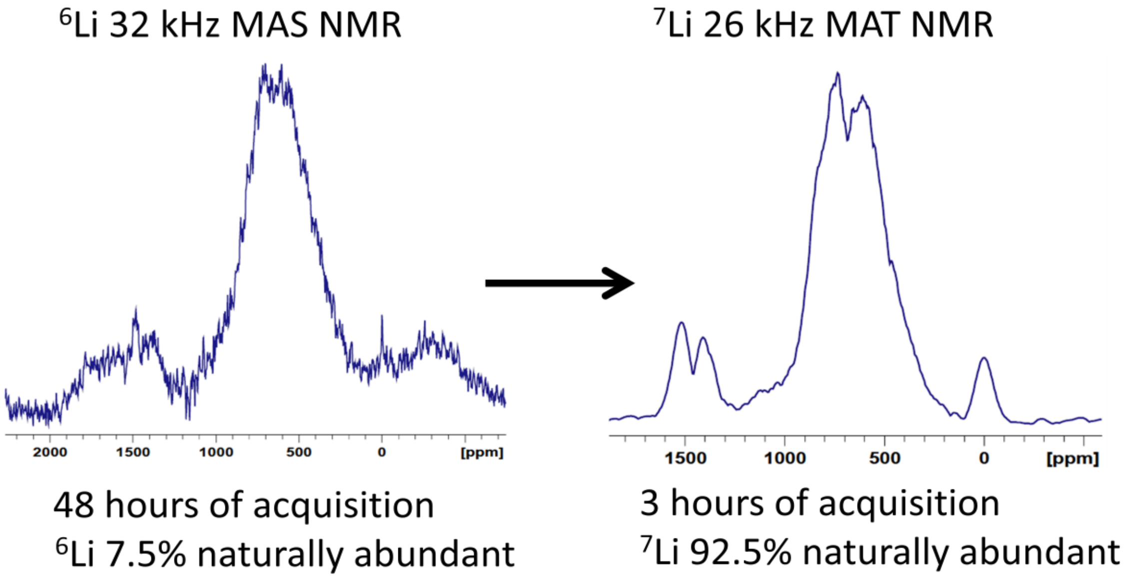

Figure 2.8 A comparison in the improvement of signal acquired using ^{6}Li with a Hahn echo MAS sequence and ^{7}Li with the MAT pulse sequence on a discharged high energy NMC sample.

However, when this sequence was used, some discrepancies were seen in the spectra of higher voltage NMC. For example, in the spectrum of 4.4V NMC (shown below), a peak at lower frequency is only observed in the ^{6}Li spectrum.

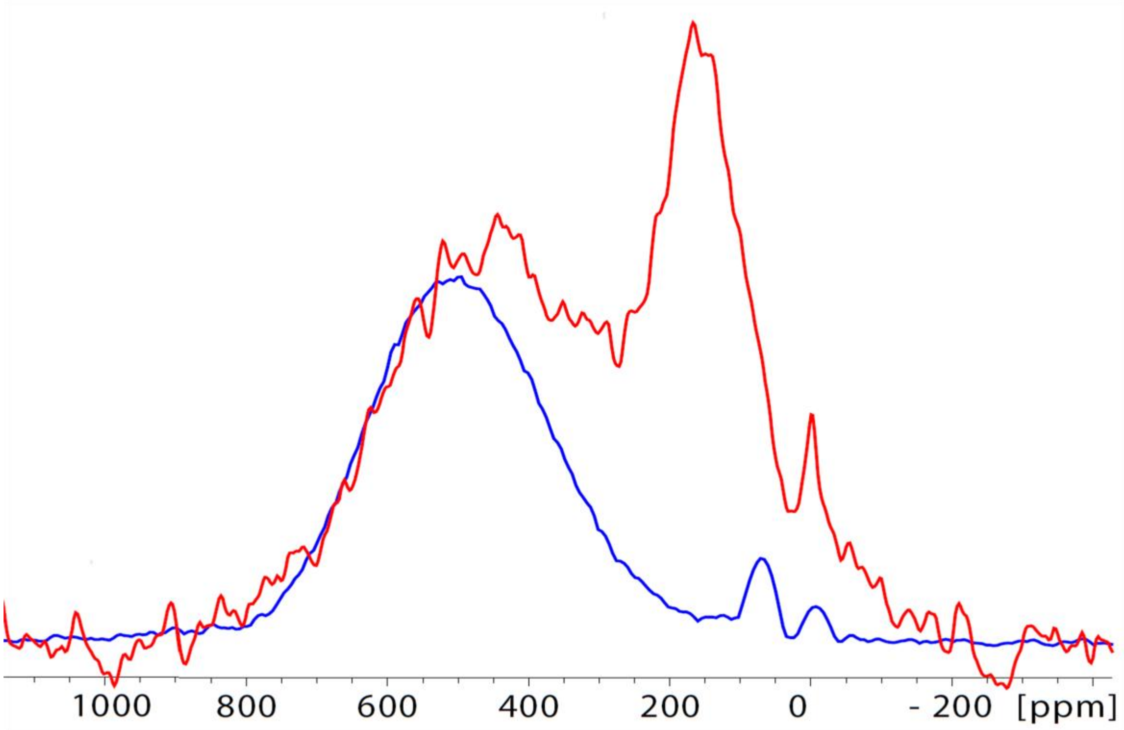

Figure 2.9 A comparison of ^{6}Li 31.5 kHz MAS NMR (red) and ^{7}Li 26 kHz MAT NMR (blue) (both in 4.7T field) of a sample which has been charged galvanostatically and potentiostatically to 4.0V.

Because of this difference, it was decided to use ^{6}Li NMR to evaluate NMC despite its low signal to noise ratio and long experimental times. It was later learned, by using fast spinning to acquire a ^{7}Li spectrum using a Hahn echo at 32 μs (acquisition at 64 μs), that this particular site has a very short T_2 and that it is likely that by the time acquisition began (~200 us after the first pulse), that this peak's intensity would have already decayed significantly. Due to the longer T_2 of ^{6}Li and shorter time before acquisition, this peak is seen in the ^{6}Li spectrum.

The ^{7}Li MAT NMR does, however, show a peak at ~70 ppm that was not previously visible beneath the ^{6}Li lineshape. This may be due to Li sites surrounded with slightly oxidized Co. In a study by Delmas et al., a signal with a shift of 57 ppm was seen for Li_xCoO_2 which drifted to ~100 ppm over the range $0.7 < x < 0.94$ [19]. Because the Co e_g band is generally thought to sit lower in energy than the Ni e_g band, this oxidation is likely due to the thermal distribution of electrons around the Fermi level oxidizing some Co below the Fermi level.

Another possibility is that it is due to the presence of 4 Mn^{4+} in the second coordination sphere of a site with 1 Mn^{4+} in the first sphere.

2.4 60 kHz MAS NMR

Acquiring a 1.3mm 60 kHz MAS probe allowed direct ^7Li acquisition. This is because the spinning speed is sufficient to push spinning sidebands beyond the main area of interest, but also, a Hahn echo pulse sequence could be done in a short enough time (64 μs) so that the lower frequency signal had not decayed as much as in MAT due to the previously mentioned fast T_2 relaxation. This provides a way to both calculate the T_2 values of individual peaks as well as gain more resolution.

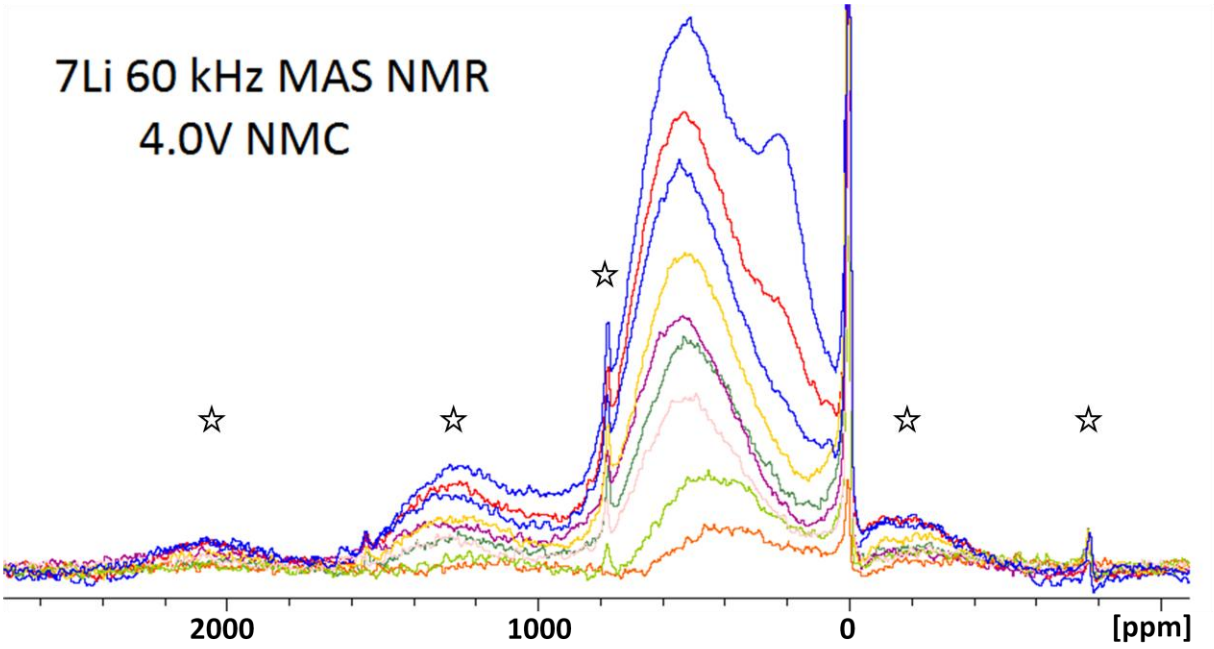

Figure 2.10 A T_2 experiment of ^{7}Li on 4.0V NMC spinning at 60 kHz in 4.7T varying the echo timing from 2 to 80 rotor periods (64 to 2560 µs after the original 90° pulse).

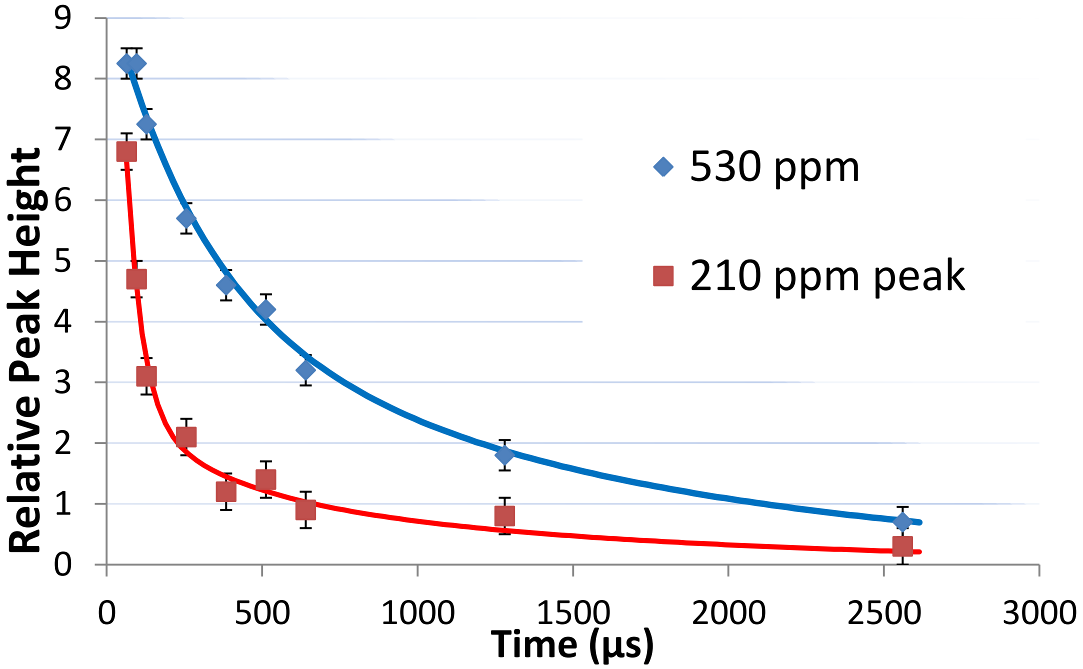

Figure 2.11 Calculated T_2 decay rates. The calculated rate for the 210 ppm peak is 50 µs whereas the 530 ppm peak is best modelled as a sum of 2 peaks which have T_2 values of 300 and 1400µs.

Not only did this give the T_2 values of the two obvious peaks (whose approximate shifts could be seen from ^{6}Li) but the shifting peak visible in the 3 longest experiments shows that there are at least 4 sites within this lineshape (including the 70 ppm peak from the ^{7}Li MAT). Including the inferred site with 3 Mn^{4+} in the first coordination sphere, this indicates more sites than the 2 and 3 that had been previously suggested in NMR experiments.[13, 31]

The ^{7}Li 60 kHz MAS NMR of 4.6V NMC (shown below in Figure 2.12) also confirms the existence of a site at 70 ppm.

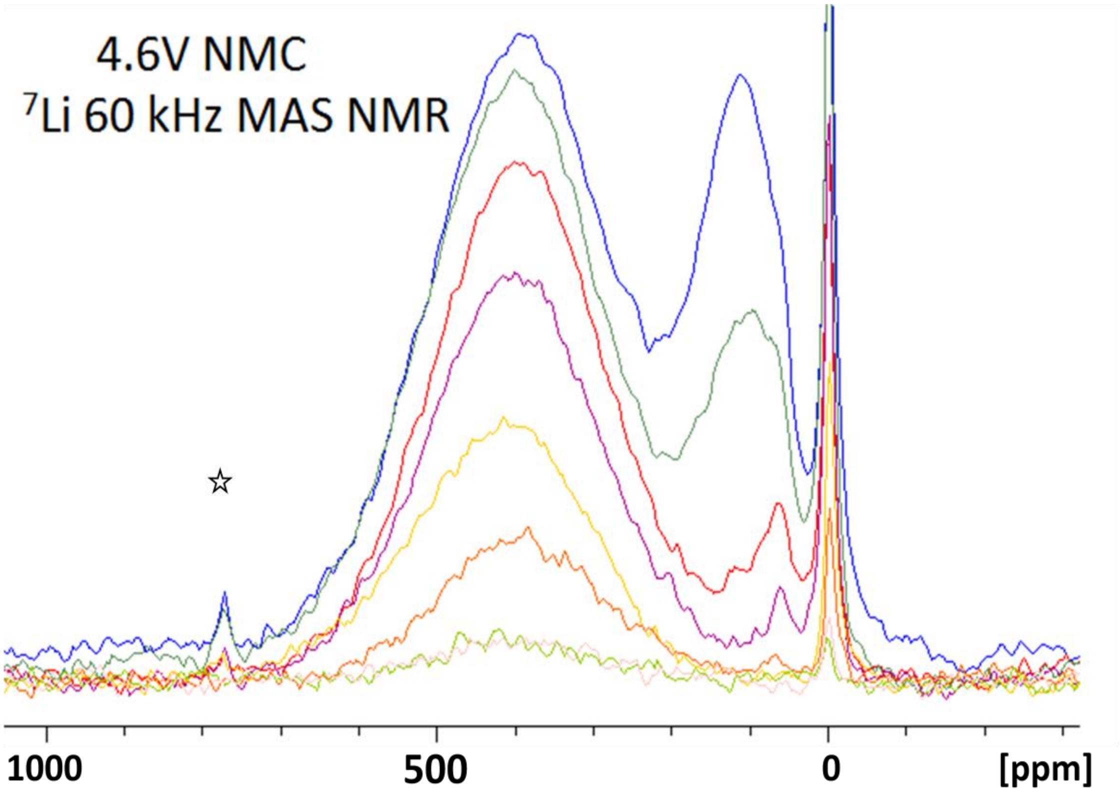

Figure 2.12 ^{7}Li 60 kHz MAS NMR of 4.6V $Li_x(Ni_{1/3}Mn_{1/3}Co_{1/3})O_2$ in 4.7T with echo timing ranging from 64 us to 3072 us after the initial 90° pulse.

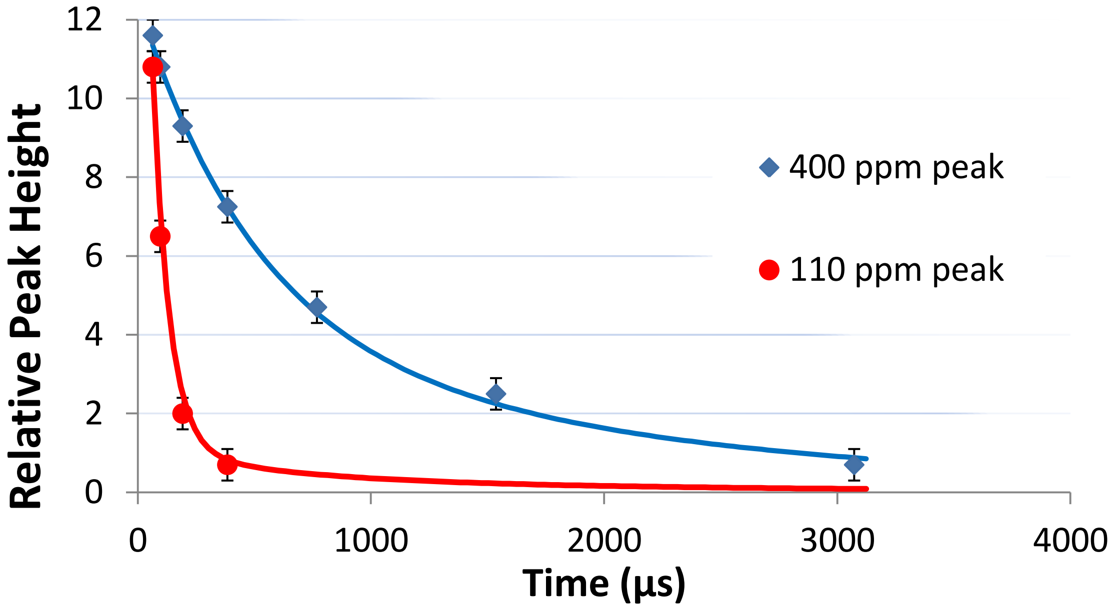

Figure 2.13 Calculated T_2 decay rates. The calculated rate for the 110 ppm peak is 70 μs whereas the 400 ppm peak is best modelled as a sum of 2 peaks which have T_2 values of 500 and 2000μs.

From 4.0V to 4.6V, the centre of mass of the 2-Mn^{4+} and 1-Mn^{4+} peaks have shifted to lower frequency by approximately 135 ppm and 90 ppm respectively. Because this shift is due to the oxidation of Ni^{2+} to Ni^{4+} (from a paramagnetic to a diamagnetic state), these shifts suggests more Ni ions in the second coordination sphere of sites that have more Mn in the first sphere. This is reasonable considering the proximity of these metals and the probable local charge balancing suggested by Zeng and Cahill.[13, 21]

It should be noted that this difference in shift on oxidation is evidence for association of adjacent Mn and Ni in the first and second coordination spheres respectively, compared to association within the entire first coordination sphere proposed by Cahill et al.[13] Though this result does not rule out charge balancing within the first coordination sphere, it can be seen in Figure 2.2 that the distance between two adjacent atoms in the first and second coordination spheres is much smaller than between the two layers comprising the first sphere. This means that the association and charge balancing proposed here is more likely, due to stronger interaction.

Additionally, on charging from 4.0V to 4.6V, the intensities of the sites associated with 2 $(Mn^{4+})^{1st}$ have decreased relative to the sites associated with 1 $(Mn^{4+})^{1st}$, meaning more Li has left these sites. This would be expected if the 2 $(Mn^{4+})^{1st}$ sites contained more Ni in either the first or second coordination sphere. Upon oxidation of this Ni, nearby Li ions would leave to balance the local charge resulting in a faster decrease of intensity for those Li sites near more Ni (the 2 $(Mn^{4+})^{1st}$ sites).

Overall, there is evidence for charge balancing; there are likely more Ni near 3 $(Mn^{4+})^{1st}$ and a relative abundance of 2 $(Mn^{4+})^{1st}$ sites. Based on our results, we can conclude that at 300°K the structure is not the highly ordered √3 × √3 30°-type superlattice which would yield only 2 $(Mn^{4+})^{1st}$ sites. This can be seen from Figure 2.14 below where each grouping of 3 transition metals contains one Mn^{4+}. Another identical transition metal layer on the opposite side of the lithium means that this transition metal structure would only yield Li sites with 2 Mn^{4+} in their first coordination sphere which we do not observe. This conclusion agrees with findings by Whitfield et al. though this structure may change depending upon the material's synthesis temperature and cooling rate.[35]

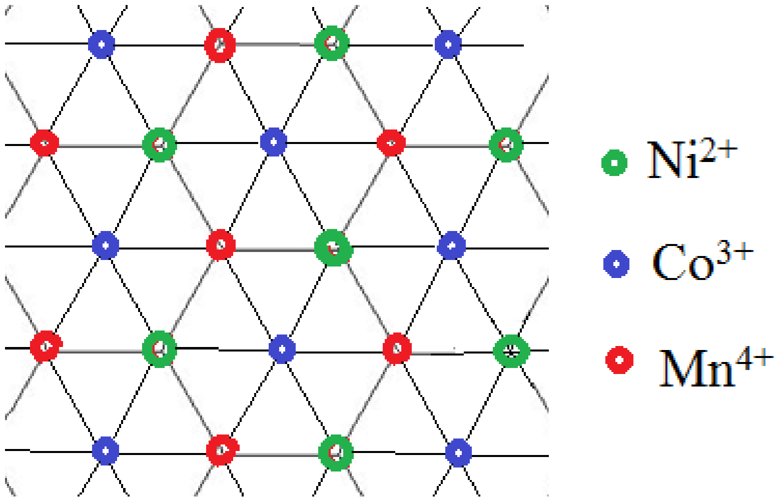

Figure 2.14 The √3 × √3 30°-type superlattice which results from complete charge balancing in a transition metal layer. This ordering is disproven by the results obtained.

2.5 Conclusions

We have evidence for the presence of a Ni conduction band which supports both previous DFT calculations and EIS results and would lend the active material good conductivity making it a good cathode material in this respect.[14, 37]

At 4.6V, we can conclude that Li resides only in sites with either 1 or 2 Mn^{4+} in the first coordination sphere. At low voltage, little can be said with certainty, however there will also be Li in sites with 3 Mn^{4+} in the first coordination sphere. Additionally, intensity at low frequencies in the spectrum of the pristine material would also suggest sites with either 1 or 0 Mn^{4+} in the first sphere. This is because Mn^{4+} and Ni^{2+} both, on the whole, contribute positive spin density to the lithium nucleus and the intensity at these lower frequencies would suggest low amounts of these metals in the surroundings.

It can also be said that Mn^{4+} and Ni^{2+} tend to neighbour, as was seen in previous studies.[21, 31] Because the Li sites with 3 Mn^{4+} in the first sphere are depopulated preferably, it may be because these sites also were near more Ni (though increased coulombic repulsion also may be a factor). This can also be seen, however, if we look at the relative decrease in the intensity of the peaks going from the 4.0V to 4.4V ^{7}Li MAS NMR spectra (below), we can say that the Li preferentially leaves the higher frequency sites. By charge balance this suggests more Ni in these sites and their frequency means that more Mn^{4+} is present, which suggests a neighbouring tendency.

Lastly, though some Ni-Mn association likely occurs, it is likely that complete order and charge balancing of the metals (as in the proposed $\sqrt{3} \times \sqrt{3}$ 30°-type superlattice) is not present. This could also be deduced from the combination of previous studies; Grey et al. showed evidence of Mn-Ni association whereas Whitfield et al. showed that no long range order exists.[21, 35] The presented results simply support these conclusions.

Chapter 3: $Li(Li_{0.2}Mn_{0.54}Ni_{0.13}Co_{0.13})O_2$

In a brief review of previous research, we know that the pristine material exhibits some long range order which is lost during the first cycle and is not regained upon discharge.[27] Oxygen is lost at high voltages on the plateau and the material likely undergoes a densification stage involving metal migration to the interior of the particles.[39,40] On reduction and reinsertion of Li, the metals are reduced to a lower oxidation state and voltage than the initial pristine material giving a larger reversible capacity than NMC.[23] Over many repeated cycles, however, lithium is no longer reinserted into the transition metal layer.[28]

While NMR studies have been done on similar charged materials as well as on pristine $Li(Li_{0.2}Mn_{0.54}Ni_{0.13}Co_{0.13})O_2$, to the author's knowledge, like NMC, no NMR studies have been performed on charged cathodes of this material which may yield structural information as they did for NMC.

3.1 Methods

The studies of HENMC were approached in a similar way to that of NMC and parallel in time so that more techniques became available over the course of the study. HENMC powder was made by colleagues at General Motors, assembled into 2032 stainless steel coin cells like those used for the NMC studies. These cells were cycled galvanostatically at a rate of C/20 to the desired voltage and transported to McMaster for disassembly and drying.

Once ^{7}Li MATPASS was implemented, coin cells were made using a HENMC powder also synthesized at General Motors in Warren, Michigan. Cathode slurries were made and cast at McMaster, left to sit for 48 hours before being cycled at a rate of C/40 due to high overpotentials. Overpotential affects the cycling of HENMC to a greater extent than regular NMC. This is because the low slope of plateau region amplifies the range of x values where the C-V curve reaches 4.6V (Figure 3.1 below). With the added (I*R) overpotential, it may reach 4.6V very early. The length of the plateau determines the amount of oxygen loss (section 1.3) and thus the stoichiometry of the material for future cycles so it is important to use low currents to keep the cycles similar.

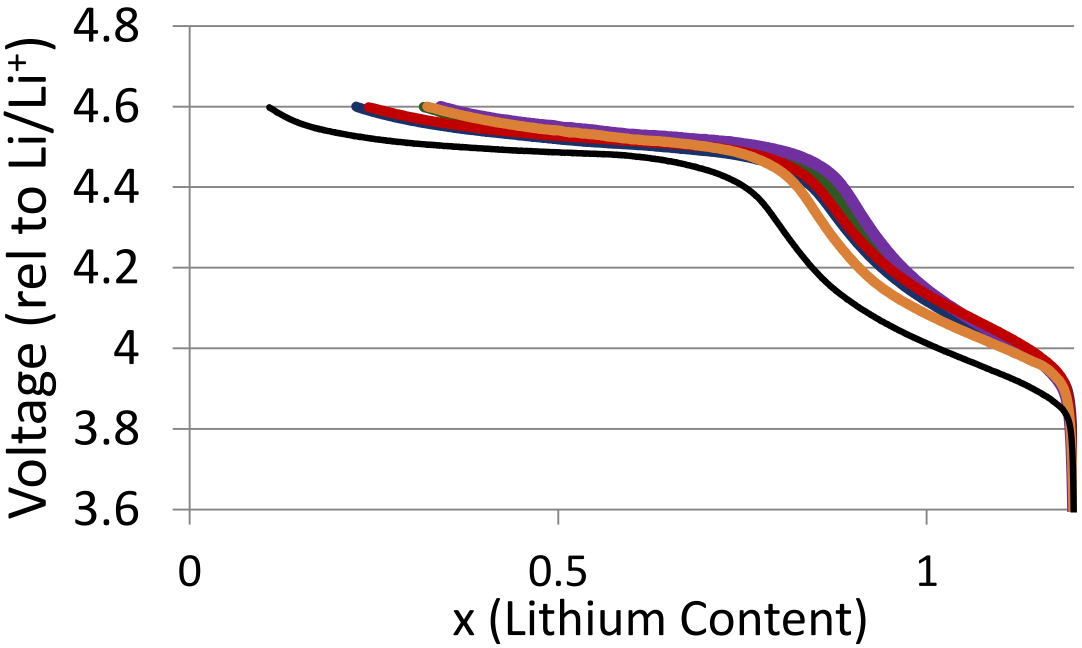

Figure 3.1 The plateau region of several of the HENMC cells showing the effect of different amounts of internal resistance. The black curve's performance is abnormal so this cathode is not directly comparable to the other cells. This cell was held at 3.8V on second discharge.

Because of the high levels of internal resistance, the cells after the first plateau were also held potentiostatically at the final voltage until the current fell to below C/100. This is except for the fully discharged cell. Its low potential of 2.0V may be beyond the potential for a phase change which was investigated by obtaining both a galvanostatically and potentiostatically discharged cell.

For the ^{6}Li MAS NMR spectra, the samples were spun at 31 kHz MAS in a 1.8 mm zirconia rotor in the 4.7T field and spectra were acquired using a 2 rotor period Hahn echo pulse sequence with a 4 μs 90° pulse and a 0.5 μs relaxation delay.

A technique called MATPASS (Magic Angle Turning Phase Adjusted Spinning Sidebands) was used. This technique is similar to MAT but only needs to collect as many spectra in the indirect dimension (slices) as there are spinning sidebands (with the full sideband intensity in that slice) thus reducing the noise collected in the many slices of MAT.[38] An example 2D spectrum is shown in Figure 3.2 and with the sidebands aligned in Figure 3.3.

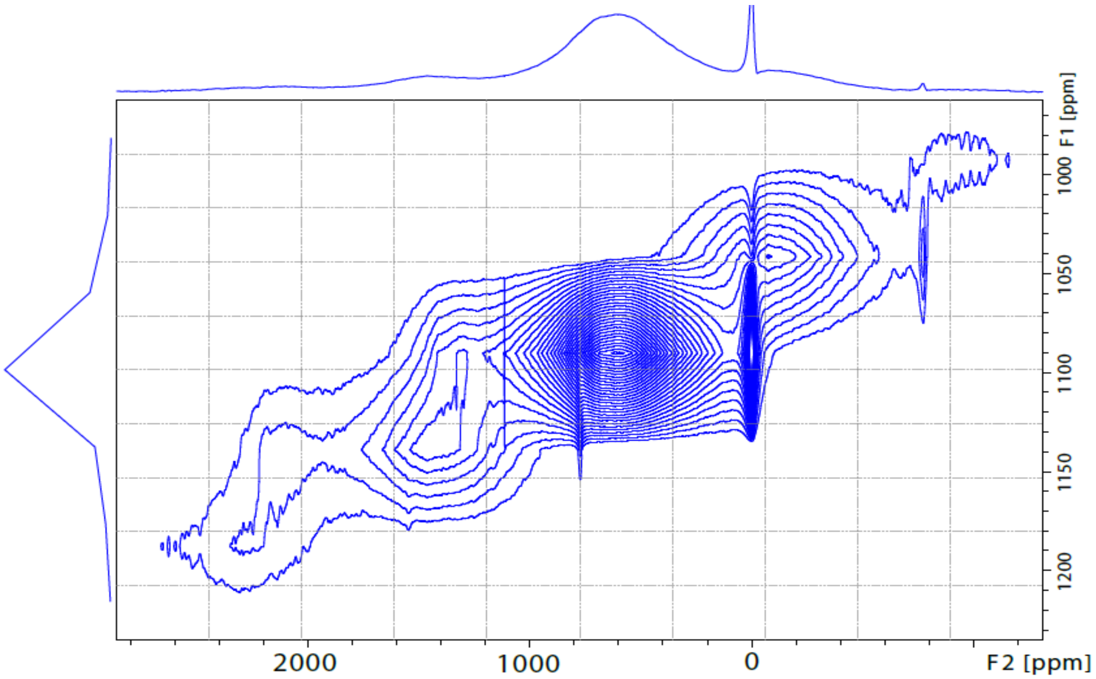

Figure 3.2. ^{7}Li MATPASS spectrum of 2.0V galvanostatically discharged HENMC in 4.7T.

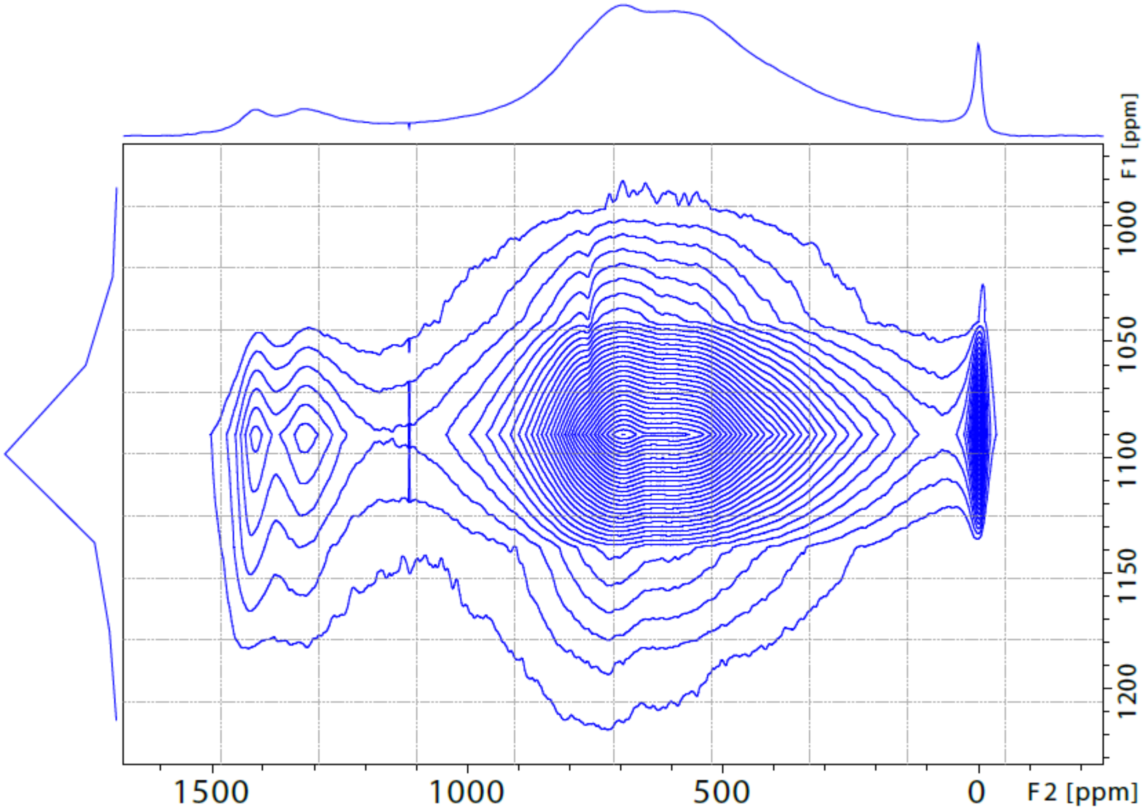

Figure 3.3. Aligned ^{7}Li MATPASS spectrum of 2.0V galvanostatically discharged HENMC in 4.7T.

All ^{7}Li MATPASS spectra were collected using a π/2 pulse length of 1.5 μs with 8 slices in the indirect dimension while spinning at 60 kHz in a 1.3 mm zirconia rotor in a 4.7T field. A 0.25 s relaxation delay was used. Because of distortions in the baseline, only the isotropic slice was selected from the acquired spectra.

3.2 ^{6}Li MAS NMR

As in the case of $Li(Ni_{1/3}Mn_{1/3}Co_{1/3})O_2$, the breadth of the isotropic peaks meant that the lowest possible field was chosen which was 4.7T. This allowed, at first, the rate of spinning to move the spinning sidebands beyond the isotropic peaks for a clear spectrum shown below.

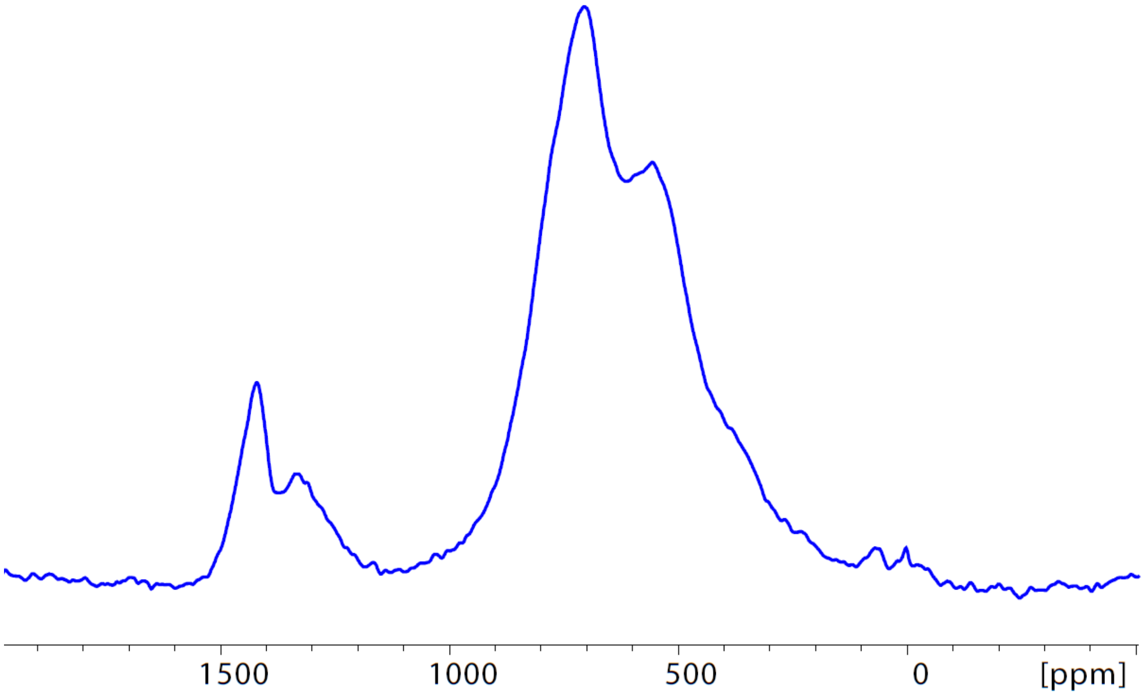

Figure 3.4 ^{6}Li spectrum of pristine HENMC spinning at 40 kHz in 4.7T field.

Table 3.1 ^{6}Li chemical shifts for elements seen in HENMC.[41]

	Mn^{4+}	Ni^{2+}	Ni^{3+}
90°	250	-30	-15
180°	-60	170	110

It can be seen that distinct peaks within HENMC are seen much more easily than in NMC. This may be due to the Li in the transition metal layer causing the "honeycomb" ordering seen in Li_2MnO_3 and observed through the low angle reflection peaks in the XRD pattern at 20-25° 2θ. It is also possible that, because of the increased amount of Mn^{4+}, some sites are far more statistically likely meaning that they form the more visible peaks.

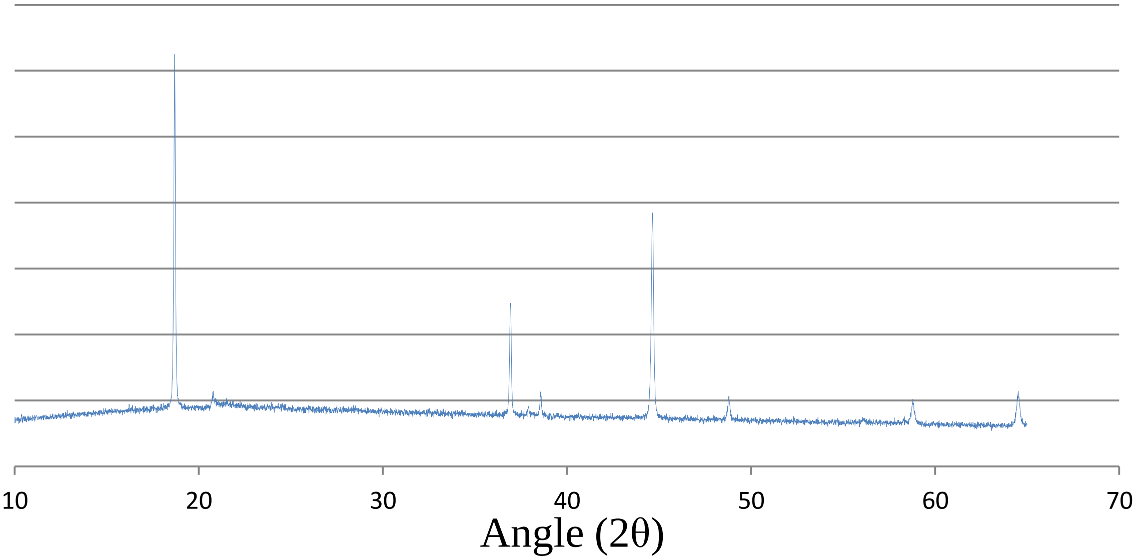

Figure 3.5 The XRD pattern of $Li(Li_{0.2}Mn_{0.54}Ni_{0.13}Co_{0.13})O_2$ obtained with Cu Kα X-rays.

In addition to the more visible Li layer peaks in the NMR spectrum, we can see a considerable amount of Li in the TM layer which would be expected from the stoichiometry. These show shifts of approximately 1420 and 1340 ppm. Shifts with similar values have been assigned to Li surrounded by 6 Mn^{4+} in the same plane and sites with 5

Mn^{4+} with either a Ni^{2+} or Co^{3+} (all interactions between Li and cations in the same layer are by 90°).[28] Upon deconvolution of the pristine HENMC, it was calculated that the TM layer only contained between 13 – 16% of the Li layer Li content. This was verified in another sample by ^{7}Li MAT NMR and may be due to the relative volatility of Li and its loss during synthesis.

3.3 ^{6}Li MAS NMR of Charged HENMC

Presented below (in Figure 3.4) are the ^{6}Li MAS NMR spectra of the samples cycled at General Motors.

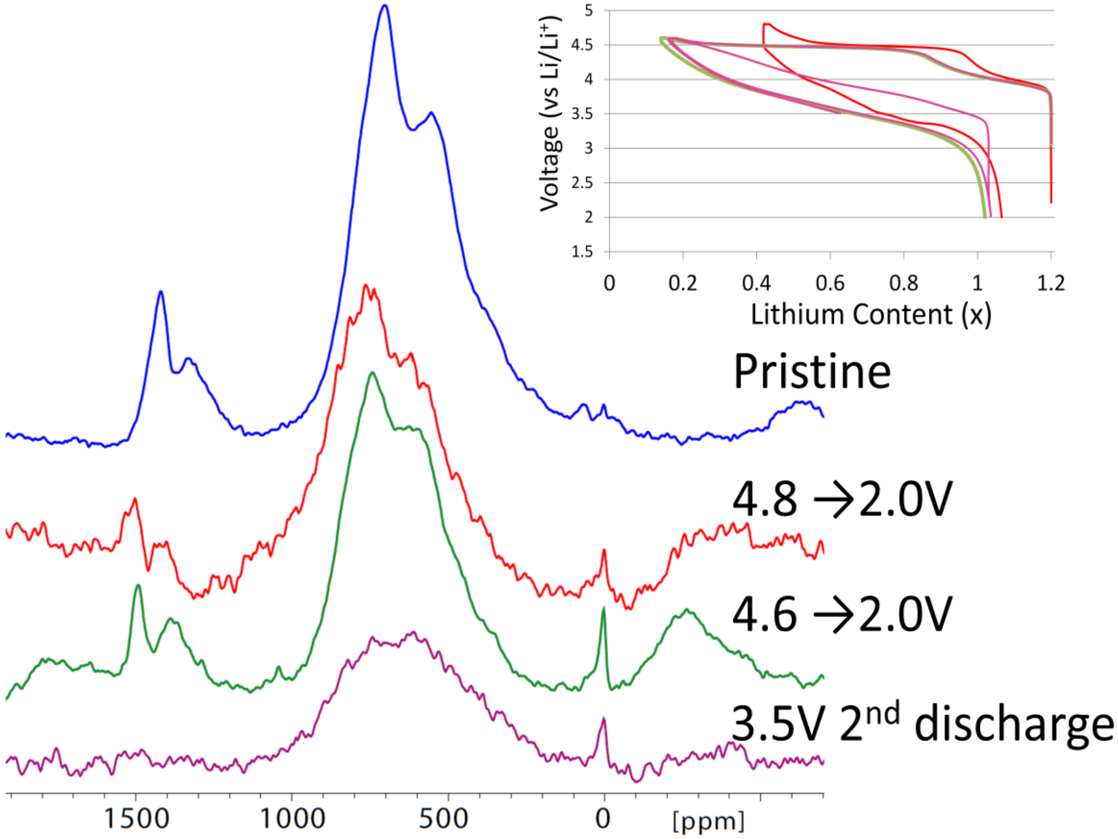

Figure 3.6 ^{6}Li HENMC spectra of cycled samples spun at 30 kHz in 4.7T. The notation 4.8 → 2.0V means the sample was charged to 4.8V and discharged to 2.0V

In the higher voltage spectrum (3.5V on 2nd discharge), because of the spinning sidebands and low S/N, it is impossible to say whether all transition metal layer Li are withdrawn. What can be concluded is that after the second discharge, there is still some Li within the transition metal layer present within the material indicating that if this Li is extracted, it can be replaced. It does appear that the transition metal layer Li intensity is slightly higher in the sample charged to 4.6V than for that charged to 4.8V suggesting the upper cutoff voltage affects the degree of repopulation. Additionally, a movement of the highest frequency peak toward higher frequencies may be indicative of either a slight rearrangement of the crystal structure or the magnetic structure of the material, either of which are certainly possible considering the densification (movement of ions) in the structure on the first charge.[39] This would require the movement of transition metal ions disrupting the crystal structure and any magnetic interaction between ions.

However, because of the lower sample mass, low natural abundance of ^{6}Li and lower spinning speeds available, the signal to noise ratio obtained after 48 hours of acquisition is poor and the overlap of spinning sidebands does not allow a clear quantification of the transition metal layer peaks. If this material is to be thoroughly evaluated, either higher spinning speeds are needed or the use of an alternate technique. Thus HENMC was a potential case for the application of ^{7}Li MAT NMR to both separate the spinning sidebands (enabling the measure of the relative intensities of the sites) and increase the overall signal.

3.4 ^{7}Li MAT NMR of HENMC

Unlike NMC, the HENMC spectrum is too wide to allow the separation of the spinning sidebands and therefore direct ^{7}Li MAS NMR could not be used. Implementation of MAT NMR allowed the separation of the spinning sidebands and a clear view of the isotropic lineshape. Unlike NMC, no differences in lineshape were noted compared to the ^{6}Li spectra obtained and separate peaks within both the Li and transition metal layer were resolved.

The samples shown below were all obtained on the second charge and discharge (during the reversible cycling seen after the first plateau cycle).

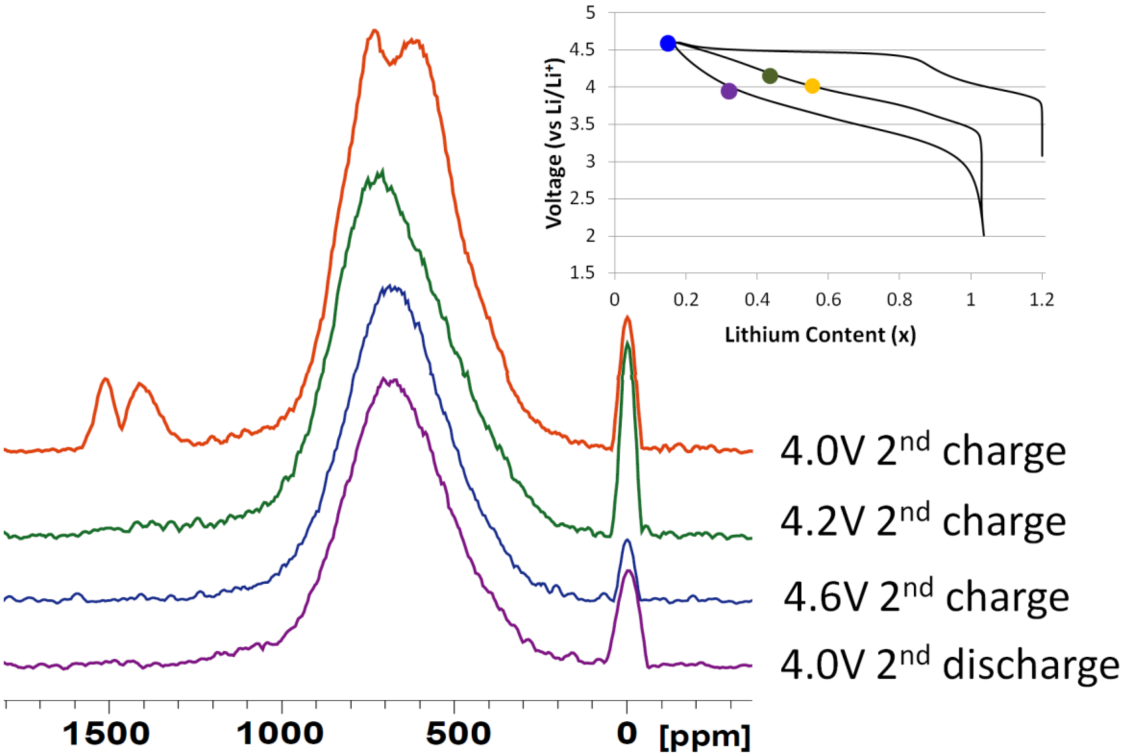

Figure 3.7 ^{7}Li MAT of HENMC cycled galvanostatically at C/20 spinning at 26 kHz in 4.7T.

Immediately visible is the lack of transition metal lithium content, which can be said with certainty at this level of signal to noise. Additionally, the lack of distinct peaks in the lithium layer region of all spectra which do not contain transition metal lithium suggests that the insertion of lithium into the transition metal layer is correlated with an ordering of the transition metals. This makes sense as the highly positive Mn^{4+} would be coulombically driven to be close to Li, whereas at high voltage, the transition metals all have similar high oxidation states (3+ and 4+) meaning there is minimal coulombic driving force for this association unlike in the pristine material. A relatively random transition metal layer would result in a more statistical distribution of the metals giving the smoother lineshape visible in the higher voltage spectra.

It should be considered that because of the internal resistance of the material and the purely galvanostatic cycling, the 4.0V sample has less lithium reinserted than even the 4.2V 2nd charge sample. Additionally, these samples had sat for several months between cycling and NMR and thus sample degradation is a reasonable concern. For these reasons, it was decided to make more cells in house whose spectra could be obtained relatively quickly after cycling.

3.5 ^{7}Li MATPASS NMR

On the Li_2O extracting first charge curve, the spectra of the beginning of the plateau (~4.45V) and end of plateau (4.6V) samples were collected and compared to the pristine material (below).

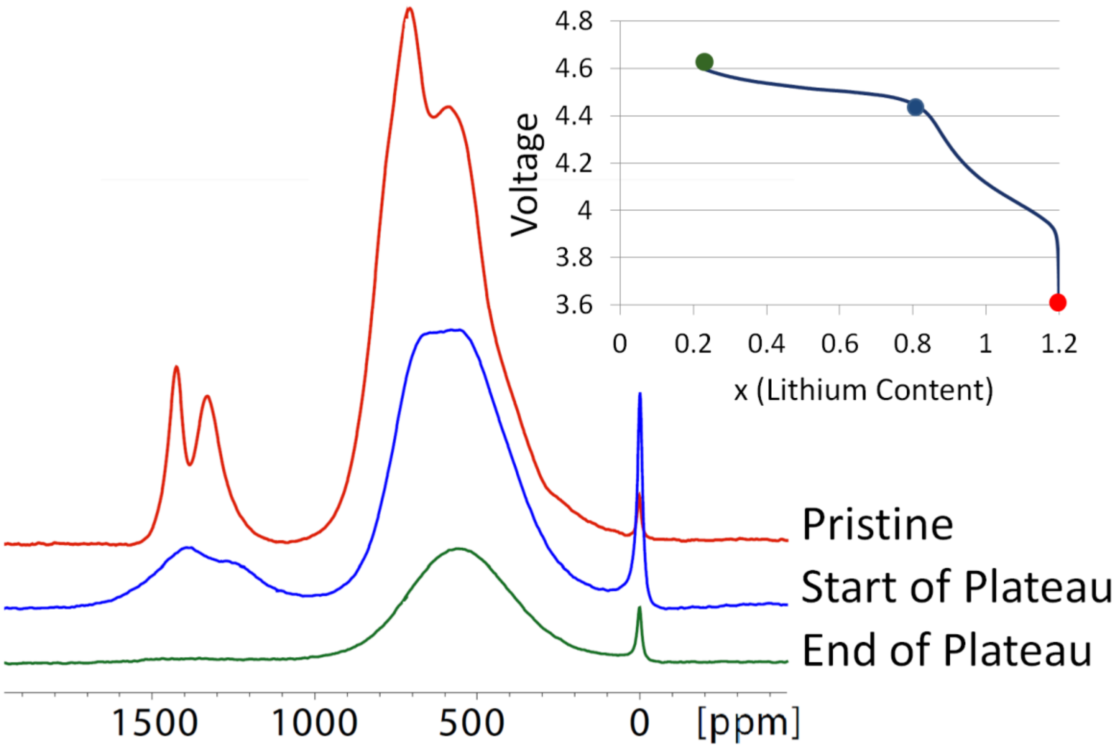

Figure 3.8 Extracted isotropic spectra from ^{7}Li MATPASS experiments on HENMC cathodes over the course of the first charge. Their electrochemistry is displayed in the C-V curve above.

The presence of transition metal layer lithium is clearly seen at the beginning of the plateau (blue spectrum corresponding to the blue point). The separate lithium layer Li peaks indicate that order is still present in the transition metal layer. Additionally, a small shift to lower frequency is observed for all peaks which one might expect to occur if Ni^{2+} is oxidized as occurred in NMC.

The increased breadth of the transition metal lithium peaks is also remarkable. The cause of this is not known though, in the future, a T_2 relaxation test may help determine whether that is the reason for the breadth of the peaks.

Upon further extraction of Li (and likely Li_2O) to the state denoted by the green mark on the charge curve, both the transition metal layer lithium and the ordering of the metals are lost from the spectrum. This is the same trend as was seen from the MAT spectra in Figure 3.6. Additionally, there is no significant change in the average chemical shift during the plateau meaning it is quite possible that all of the metals retain the same charge as at the beginning of the plateau as was suggested by Dahn et al. by XRD.[22]

Over the second discharge (during reproducible cycling), cathodes at several voltages were extracted from the cells and their ^{7}Li MATPASS spectra were obtained as shown below in Figure 3.7.

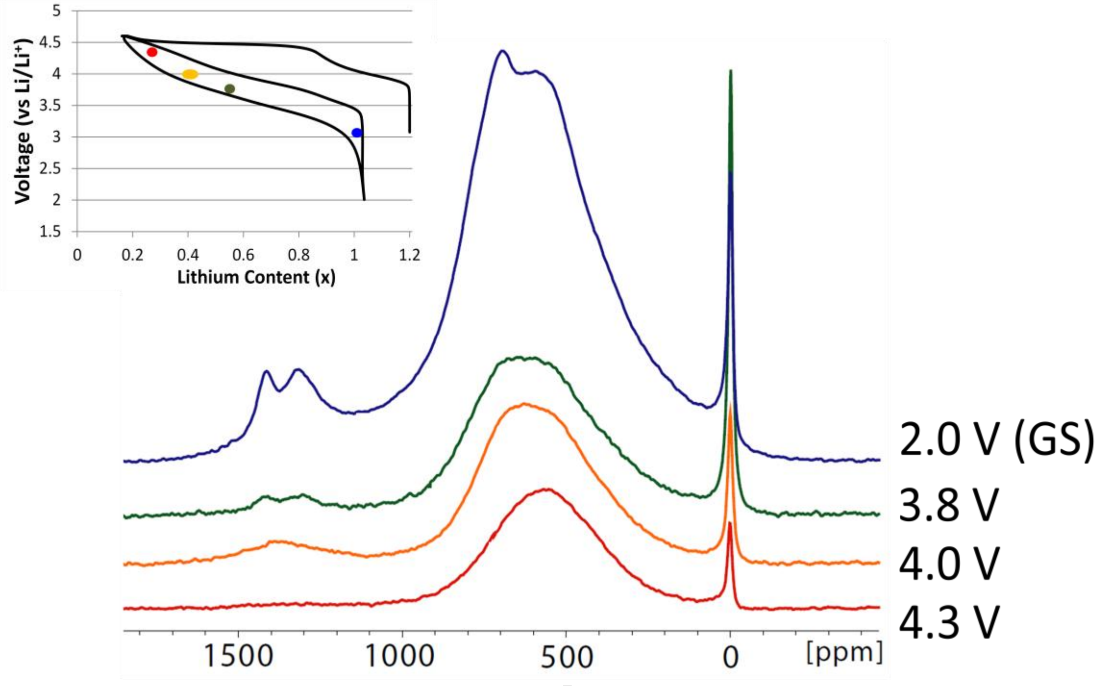

Figure 3.9 Extracted isotropic spectra from ^{7}Li MATPASS experiments on HENMC cathodes over the course of the second discharge.

It can be seen from these cells that transition metal layer Li was returned on the second discharge as it was on the first. The trend of the material experiencing shifts to higher frequency as the transition metal layer lithium ions are returned is also seen in this sample as it was in the MAT spectra of the 2nd cycle.

It should be noted that the 3.8V cell experienced a significantly longer plateau during the first charge meaning that it contains less Li than would be expected. When the electrochemistry for this cell is considered, it has an x value of 0.25 whereas the 4.0V Li sample has an x value of 0.3 Li. While being non-ideal because due to the longer plateau, the comparison of these spectra suggest that transition metal layer lithium content is dependent foremost upon the voltage (oxidation state of the transition metals) rather than upon the lithium content. This is understandable considering transition metal layer sites would be preferable when the nearby ions are in reduced states minimizing the coulombic repulsion. This point is strengthened when one considers that according to the densification model, the 3.8V sample would have even fewer sites for Li in the transition metal layer and yet has more defined peaks for Li in these sites.

Another point of interest is that there appears to be less intensity for the transition metal layer Li upon galvanostatic discharge to 2.0V than in the pristine material (shown below). This may be because densification of the material has led to there being fewer sites for transition metal layer Li after compression of the structure.[39] When this spectrum is deconvoluted and the intensities of the peaks compared, it was found that Li in the TM layer was decreased in amount (75% of that in the pristine material) as well as in ratio to the Li layer Li which are reinserted (approximately 10% compared to 15% in the pristine material). This supports the densification model wherein transition metal layer Li are lost as transition metals migrate and occupy Li sites.[39]

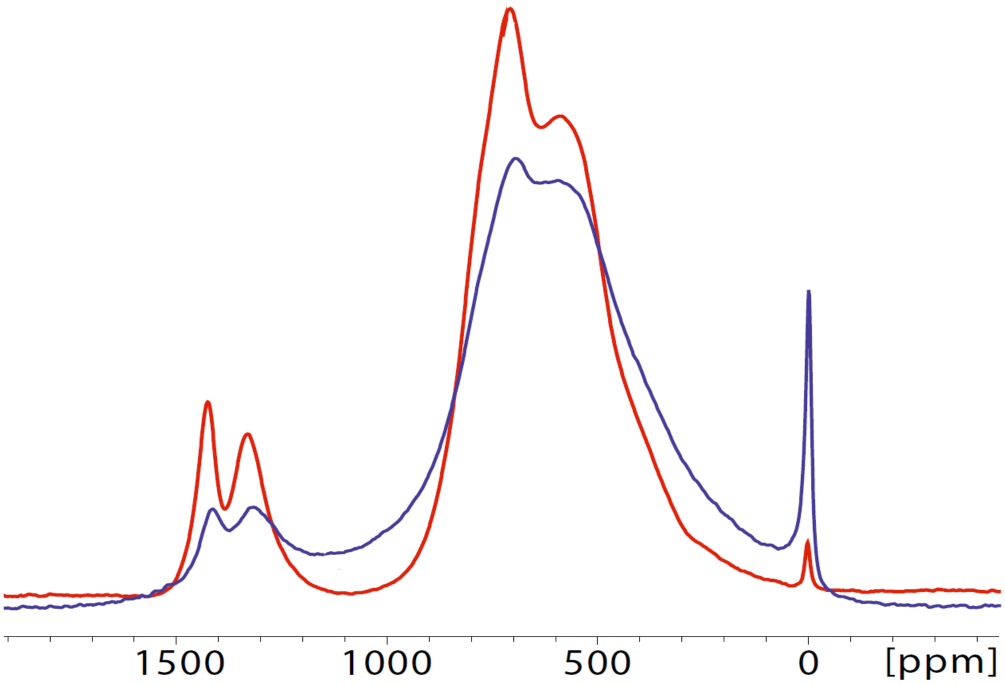

Figure 3.10 Pristine ^{7}Li MATPASS isotropic spectrum (blue) and 2.0V 2nd galvanostatic discharge (red) showing the reduced intensity of transition metal layer lithium.

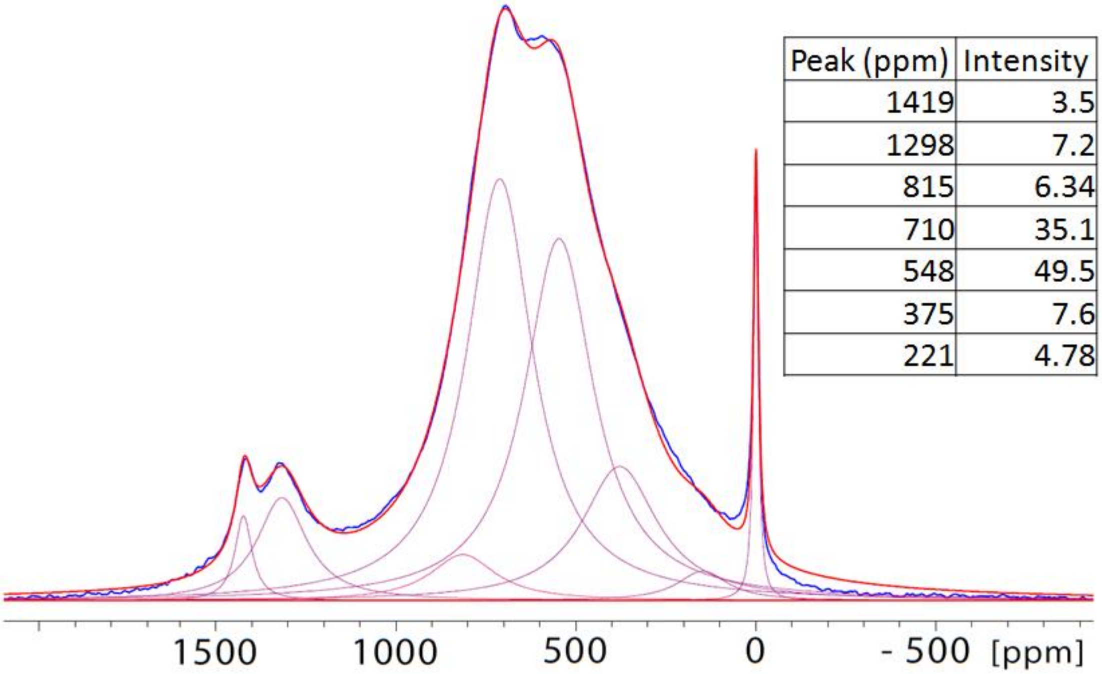

Peak (ppm)	Intensity
1419	3.5
1298	7.2
815	6.34
710	35.1
548	49.5
375	7.6
221	4.78

Figure 3.11 Deconvolution of the ^{7}Li MATPASS spectrum of 2.0 V galvanostatically discharged HENMC in 4.7T. The sites shown are not definite but used to calculate amounts of lithium.

Also evident in this spectrum is the increase in intensity at frequencies previously unseen (the 900 – 1200 ppm range). There are at least two likely reasons as to why these frequencies are now present. Firstly, it has been supposed that on the plateau, the path of least resistance for metal migration is through the Li layer.[39] If Mn^{4+} remained to some extent in the Li layer during lithium reinsertion, it would contribute a shift of 250 ppm to the six Li nearest it giving several Li-layer Li a higher frequency than they had before.

Another option, which is not mutually exclusive with the first, is that because of transition metal rearrangement upon Li ion extraction, a more statistical distribution of transition metal ions is created. This, when combined with the densification which increases the content of paramagnetic ions in the transition metal layer, may create more cases with 4 $(Mn^{4+})^{1st}$ leading to shifts in excess of 1000 ppm.

The width of added intensity may be accounted for in that is quite possible that due to partial Mn reduction in combination with its abundance in this cathode, this material becomes a hopping semiconductor.[42] If several Mn surround a Li atom and each could be in a 4+ or 3+ oxidation state, the chemical shift of Li could vary quite significantly resulting in the broad region that we see.

Another comparison that can be made for discharged samples is between galvanostatically and potentiostatically discharged samples. The difference between these cells can be seen immediately from the electrochemistry shown below.

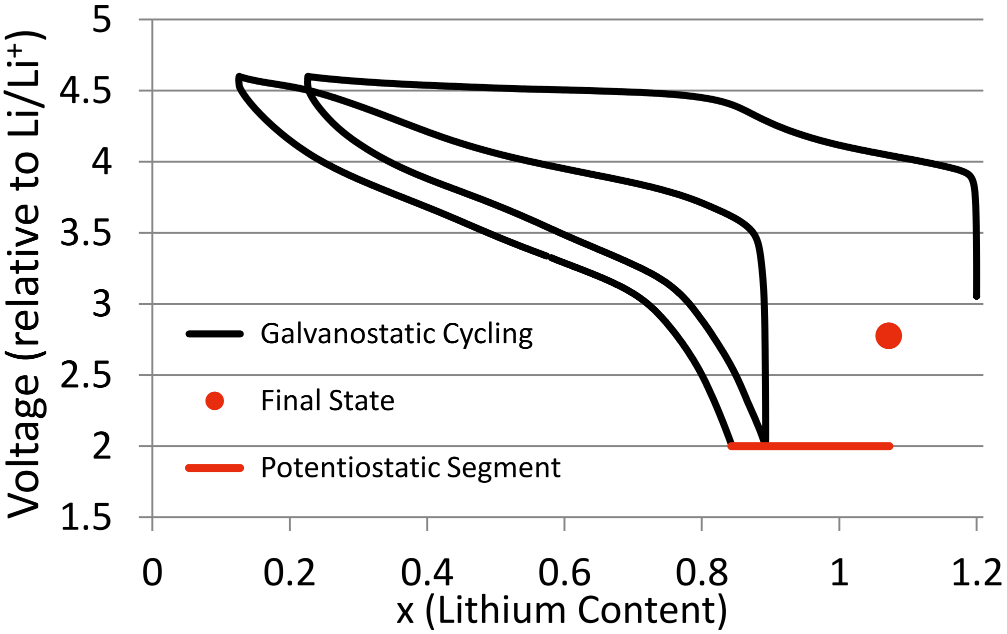

Figure 3.12 The electrochemical curve of the 2.0V galvanostatic 2nd discharge sample with the added capacity achieved by the potentiostatic discharge. Note that the added capacity was not sufficient to bring the cell to 2.0V and the cell relaxed to 2.78V. The galvanostatically discharged sample relaxed to 3.37V.

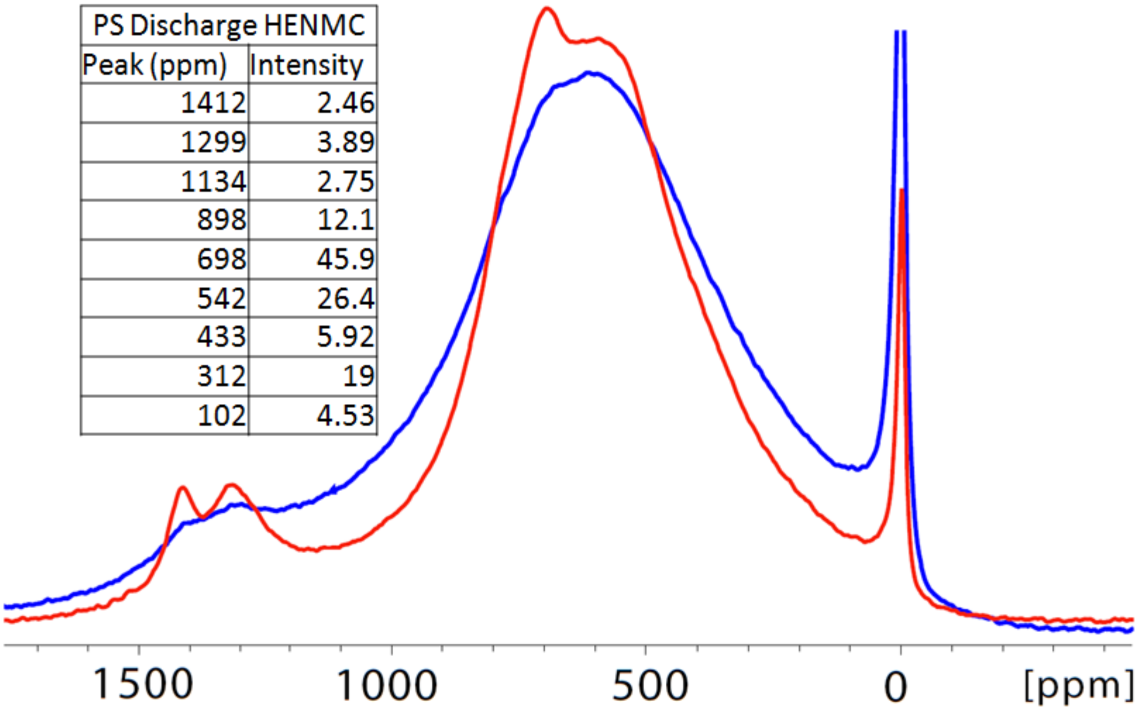

PS Discharge HENMC	
Peak (ppm)	Intensity
1412	2.46
1299	3.89
1134	2.75
898	12.1
698	45.9
542	26.4
433	5.92
312	19
102	4.53

Figure 3.13 The ^{7}Li MATPASS isotropic spectra of the galvanostatically (red) and potentiostatically (blue) 2.0V discharged samples spinning at 60 kHz in 4.7T.

By the increased intensity above and below the lithium layer peaks as well as the loss of definition in the lithium layer peaks and transition metal layer peaks, we can say that there is some significant change in the material. This may be a phase change or a reduction of one of the transition metals. Mn^{3+} which has been shown to be present in the reduced materials, contributes a much smaller positive chemical shift than Mn^{4+} which may account for the increased intensity at low frequencies.[8, 23]

The gained intensity at ~1000 ppm is at the high end of the Li chemical shift range for Li in tetrahedral sites of Mn^{4+} spinel phases which are believed to be formed at ~3.2 V.[8, 23] This would explain the intensity increase in these regions for the sample which was held at 2.0V longer. This hypothesis is strengthened by the observation of spinel on the edges of the particles of active material by TEM. An interesting feature of this spectrum is that it contains only 40% of the intensity in the typical transition metal layer lithium frequencies as the galvanostatic spectrum. Given the higher energy of these sites, it is possible that they contribute preferentially to the formation of the spinel structure.

For the Li in the transition metal layer, the action of the hopping semiconduction could mean that all 5 or 6 Mn could be in either a 4+ or 3+ oxidation state for each scan. When combined with increased reduction of Mn^{4+}, this would decrease the observed frequency (relative to the pristine material) as well as broaden it. This would account for the apparent decrease in transition metal layer Li intensity. It would also account for the broadening of the lineshape in general.

3.6 Long-Term Cycling

Because the material must be able to cycle many times with good capacity retention to be a feasible material for use in vehicular applications, a long term cycling experiment was performed. A coin cell was cycled 50 times by colleagues at General Motors and the cathode was extracted. Shown below are the ^{7}Li MAT NMR spectra of pristine HENMC and the 50 cycled sample.

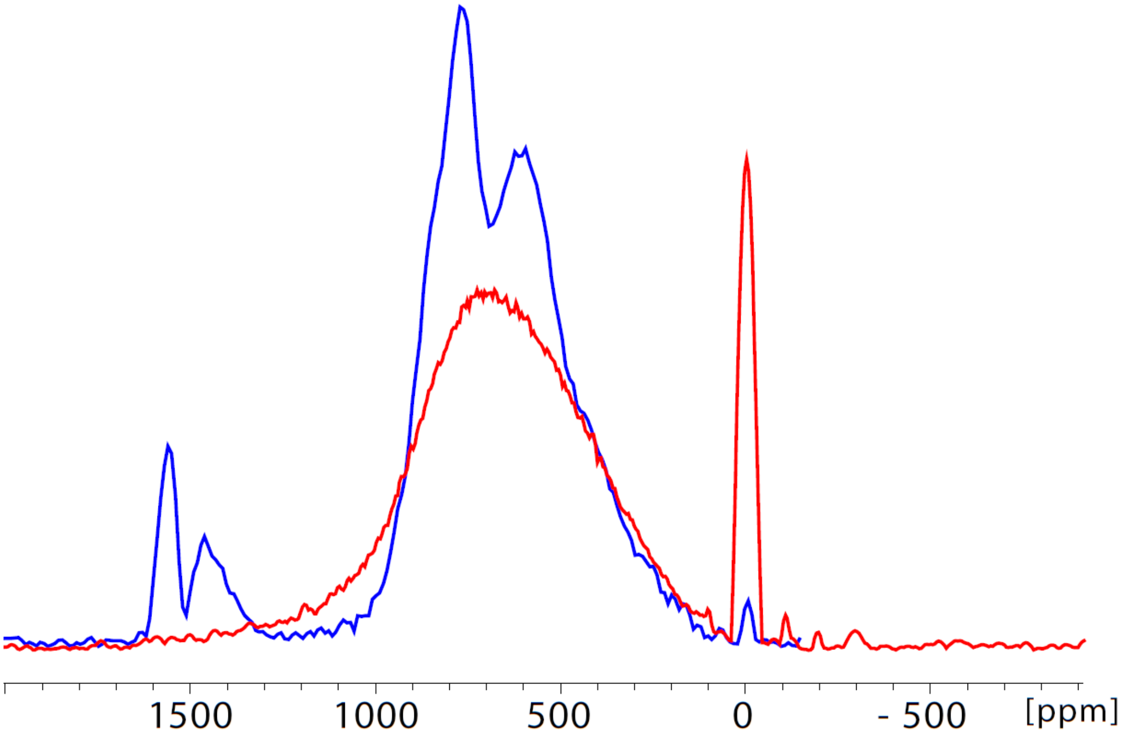

Figure 3.14 ^{7}Li MAT NMR in 4.7T of a cathode which has been cycled 50 times between 4.6 and 2.0V (red) compared to the pristine material (blue).

The spectrum of the 50 cycled samples clearly shows that the cathode has little to no lithium in the transition metal layer and that the metal ions are disordered. This is in agreement with results for similar materials in literature.[27] It may be the case that the material underwent further densification removing the transition metal layer Li sites or that these Li are less thermodynamically stable than in the spinel phase which has been shown to slowly form during extended cycling.[43] Thus they would become part of the spinel phase and contributed intensity at lower frequency.

3.7 Conclusion

The results that have been obtained by both ^{6}Li and ^{7}Li NMR agree well with current literature regarding similar materials. Transition metal layer Li are reinserted into the material after the first and second charge though are slowly unable to be reinserted or join the spinel phase. The removal of the transition metal layer Li causes disorder of the transition metals and the lower amount of transition metal layer Li reinserted supports the densification model.[39] There is also evidence of change in the discharged material either of a spinel phase formation or Mn in the Li layer by the increased intensity at ~1100 ppm. Finally, deep discharge (potentiostatic) of the material causes significant change to Li environments prompting more investigation which may provide a functional limit to lower voltage.

Chapter 4: In-Situ NMR

4.1 Motivation

Typically, electrochemical-NMR experiments have been carried out *ex-situ*. This means that a cell is charged/discharged to a certain point, disassembled in a glovebox, the component of interest is dried (often for several hours), packed into an NMR rotor and spun. In contrast, *in-situ NMR*, as it pertains to batteries and the components thereof, means acquiring spectra during the application of current. Thus *in-situ* NMR gives the advantage of being able to acquire data at several states of charge much faster than if the cell must be disassembled and the component dried before acquisition, which requires more time. Additionally, if morphology or physical parameters are being investigated, *in-situ* NMR allows the components to be in the same condition, in general, as they would be in practice without complicating factors such as the effects of drying and lack of liquid electrolyte.

However, one of the most valuable reasons for *in-situ* data acquisition is that phases can and have been detected which are not seen in *ex-situ* studies. In 2008, Grey et al. studied silicon electrodes using both *ex-situ* and *in-situ* techniques and upon cycling, they observed a new peak which contributed about half the intensity of the ^{7}Li spectrum [44]. If these phases exist within cells during typical cycling, it is important to know about them and how they affect cells' performance; do they impede ion motion, do they induce strain in the material?

4.2 Obstacles in *In-situ* NMR

There are, however, inherent difficulties in creating a cell to operate and yield an interpretable signal within the magnetic field of a spectrometer and the probe. One significant difficulty is an electrochemical cell cannot be spun in a rotor easily. Because spinning is often done in excess of 1 kHz, the centrifugal forces on the cell would likely lead to separation of the components and damage. Conducting experiments statically on solids means that the CSA will not be averaged leading to broadened resonances. If the CSA is large, overlapping peaks can lead to difficult interpretation if many individual peaks are present, as in NMC.

Similarly, dipolar coupling within a cell is not averaged in static samples. Materials with unpaired electrons, whether conductors with unpaired electrons at the Fermi level or paramagnetic metal oxides, can exhibit greatly varying shifts dependent on their shape and orientation (as explained in chapter 1) and even multiple shifts depending on the nucleus's location within the particle.[41] The dipolar shift contributed to any one nucleus can be obtained from summing the contributions from every other unpaired electron within the sample.

It is then seen that within a sample, different shifts result. For example, a nucleus near the edge of a sample is a greater average distance from the dipoles of the electrons and will lack some of the shift seen for nuclei in the bulk which are surrounded by dipolar fields. For samples with one axis much larger than the others, the dependence of dipolar coupling on $3\cos^2\theta - 1$ is seen clearly as the sample is rotated relative to the magnetic field. In the case of a thin film of $Li_{1.08}Mn_{1.92}O_4$ in a magnetic field pointing up, this resulted in a shift ranging between -117 (horizontal) to 803 ppm (vertical) and for Li metal, a shift of between 244 ppm (horizontal) and 272 ppm (vertical).[30] This is clearly significant and must be taken into account during *in-situ* experiments.

The skin-depth penetration of RF radiation must also be taken into account when designing *in-situ* cells. This is the name given to the exponential decay of the intensity of the radio frequency magnetic field within a conductive material [30]. This decay of intensity is due to induced currents within the material creating opposing magnetic fields which cancel the applied fields. It was predicted that the magnitude of these opposing fields, and thus the distance of penetration, would be dependent on the electrical resistance of the materials, the magnitude of the applied field and the frequency of the applied field. This is reflected in the equation for the radiation intensity

$$\omega_1(x) = \omega_1 e^{\frac{-x}{d}} \quad \text{where} \quad \text{d is the skin depth and is given by } \frac{1}{\pi\mu_0}\sqrt{\frac{\rho}{\mu_R f}}$$

where ω_1 is the intensity of the radio frequency magnetic field, x is distance, ρ is the resistivity of the metal, μ_0 is the magnetic vacuum permeability, μ_R is the relative permeability of the metal and f is the applied frequency [30].

In the case of a typical coin cell, where both lithium metal and Al foil are present near the materials of interest, the active opposing fields can potentially extend over the material reducing the effective B_1 field. This can be constraining if a large bandwidth is desired and the power of the probe is limited. Additionally, the precessing magnetic field from the nuclei induce the same effect in the metals which reduces the signal that can be acquired. It was calculated that the skin depth penetration of Al for an applied frequency of

77 MHz would be 10 μm [30]. As typical Al foil used in our experiments is about 31 μm thick, very little magnetic field would penetrate.

The potentially reduced signal brings up another concern which is the addition of spectra. In *ex-situ* NMR, many scans can be collected which all represent the same point on a capacity-voltage curve. However, in *in-situ* NMR, each scan is taken from a slightly different point and they must be combined. This leads to a compromise between signal to noise ratio, C-V curve accuracy and cycling rate which must be chosen depending upon the information desired.

4.3 Previous *In-situ* Cell Designs

The first *in-situ* electrochemistry was performed by Rathke et al. on polymer electrolytes to measure concentration gradients.[45] Later, the same group conducted experiments involving the insertion of Li into carbon.[46] The cell mimicked a 2032 coin cell with an exterior made of teflon using one of the electrodes as part of the NMR detection circuit. However, this cell suffered from low signal to noise.[30]

The Letellier/Tarascon group has since been one of the most active groups in the field of *in-situ* NMR. In many of their experiments, they used a laminated plastic Bellcore type cell. In this design, rectangular pieces of a free standing cathode (no aluminum backing), separator and lithium metal are placed between two long pieces of copper mesh (with holes to allow the B_1 field to penetrate the active material). This requires a device to laminate at 130°C and 25 psi inside a glove box. This cell was cycled within a solenoid so that the B_1 field is in the plane of the thin cell and provided adequate signal to noise for a detailed spectrum when cycled at a C/20 rate.[47]

Later, in 2011, the Letellier/Tarascon group changed to a cylindrical polypropylene cell. This design, shown below in Figure 4.1, gave several improvements over the thin laminated cell and was used in a solenoid coil.[48]

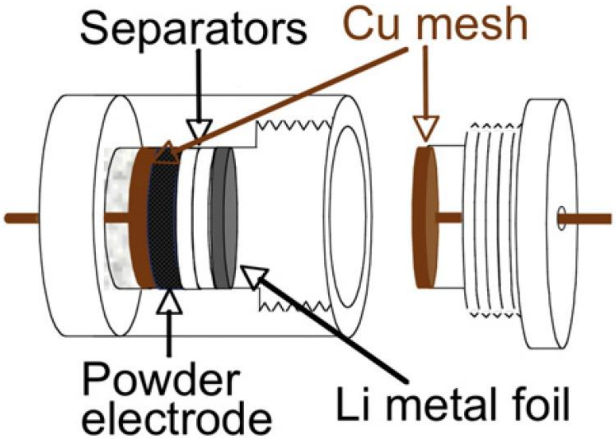

Figure 4.1 The Letellier cylindrical cell used to investigate cathode materials.[48]

This design reduces the area that needs to be hermetically sealed compared to the laminated cell and can maintain pressure better than the laminated plastic cells. This cell also allows the use of up to 4 times the active material of the laminated cell and results in approximately 8 times the signal to noise due to an improved fill factor.

However, the use of metallic components decreases the signal by about two thirds. Additionally, it does not include a spring and does show an increase in internal resistance which becomes significant after two cycles.[48]

4.4 *In-situ* Cell Design

The original cell design, shown below, was intended to reproduce Letellier’s design. It was hoped to see if the cell could be cycled at the high rates which might be seen in vehicular applications and be modified to maintain pressure within.

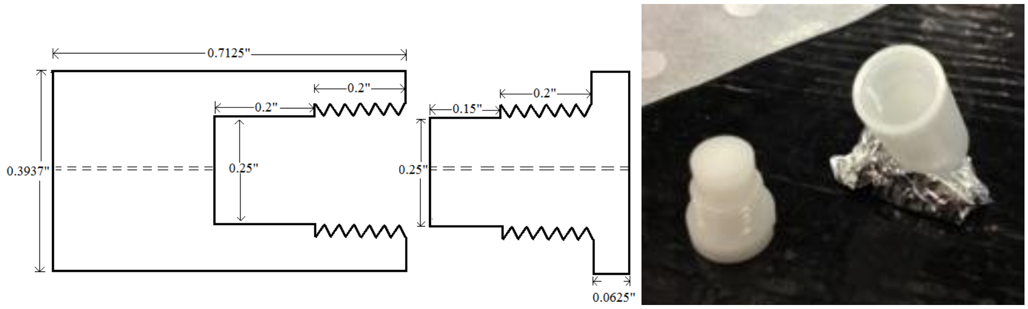

Figure 4.2 Original *in-situ* cell design mimicking the Letellier design.

The drawbacks of this cell design was the difficulty in making electrical connections to copper within the battery, the high manufacturing cost, difficulty in making a seal and poor cycling results. The poor cycling may have been due to several factors. Firstly, the defined distance between the plastic parts may have lead to insufficient compression if the lithium metal was rolled too thin. Another possibility is that the twisting motion from threading the cap in may have abraded the cathode and either damaged the cathode or the electrical connections.

For these reasons, it was then decided to use a Swagelok type cell. This cell, pictured below, is made of Teflon and consists of a Swagelok union piece with two cylinders which have a channel through the centre for a wire to connect to each electrode. The centre has been drilled to a set diameter (0.25”) and the outside milled to accommodate the coil.

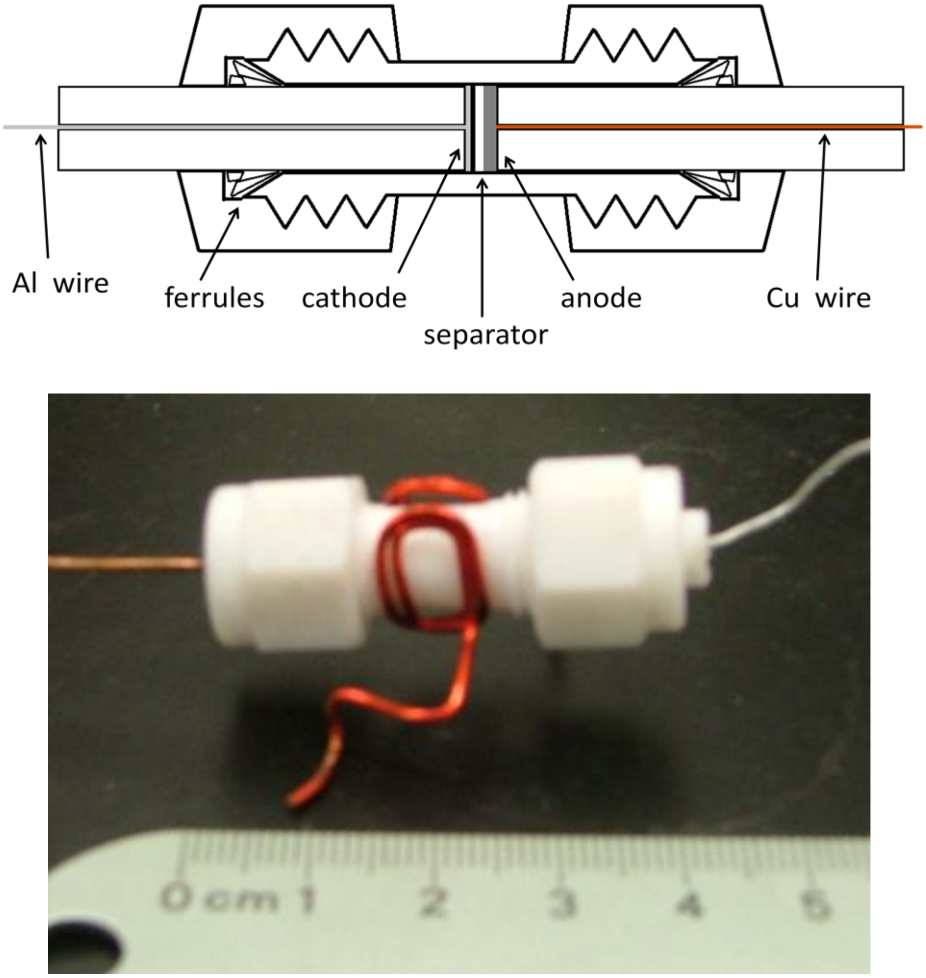

Figure 4.3 Teflon Swagelok cell design (above) and actual cell with saddle coil (below).

To assemble the cell, the cathode cylinder, with Al wire and Al current collector, is inserted with the ferrules surrounding it. The cathode is then inserted, then electrolyte, then the desired number of separators with electrolyte following each (often two separators are used to prevent an internal short). Finally, a disk of Li metal is inserted with electrolyte and the other Teflon cylinder is inserted and compressed. This allows excess electrolyte to exit via the diameter difference of the drilled hole for the wire and the wire itself. Finally, the caps are screwed on tightening the ferrules and forming a seal around the cell. Parafilm, with vacuum grease, is used to seal the channels for the wires.

This cell offers the advantages of allowing compression regardless of the number of separators, no torsion of the cell components and it can be easily manufactured in-house which significantly reduces the cost. It also shows significantly improved electrical performance (shown below), when tested with a $LiCoO_2$ cathode, which may be a result of these factors. This should allow cycling at higher rates than have been seen in literature and which may allow easier detection of metastable phases.

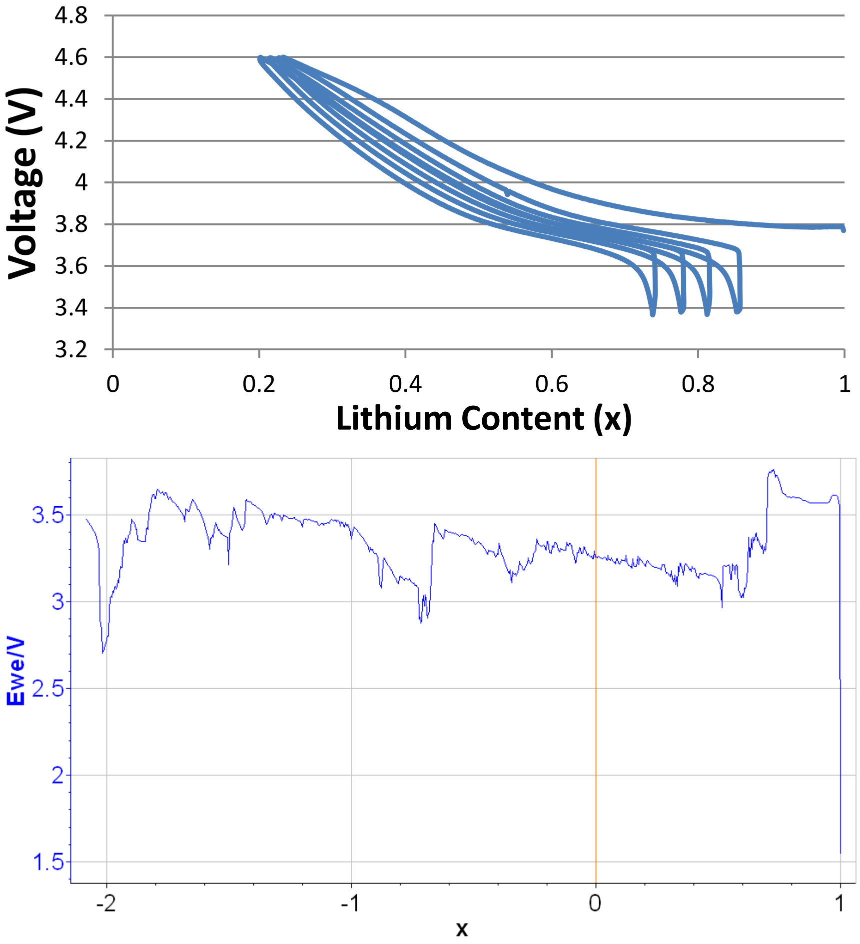

Figure 4.4 Electrochemical profile of NMC in the Teflon Swagelok cell (top) and the Letellier-like design (bottom).

Another modification to the design of the cell which could have been implemented in the previous cell was the electrical connection to the cathode. This was done by hooking Al foil to the wire as shown below. The hook sits in a depression in the Teflon cylinder while the foil extends out to contact the back of the cathode. This is easier to assemble and would also result in less strain on the cathode than the wire knot in the Letellier cell.

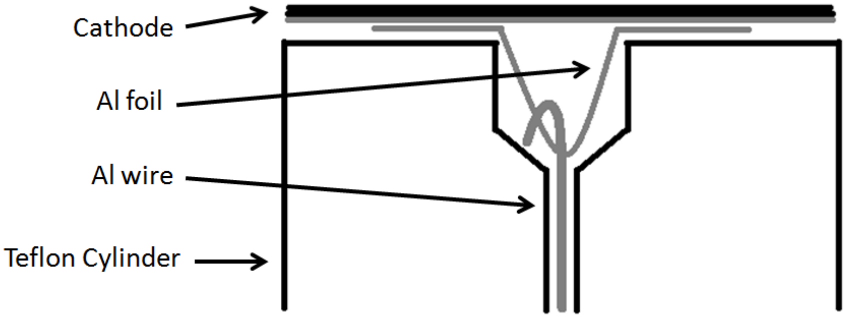

Figure 4.5 The aluminum wire hook and connecting foil to form a solderless contact.

When conducting NMR of a cathode cycled within the cell however, little to no signal was observed using a solenoid coil. Letellier had observed signal from his cell which used a copper mesh as a current collector.[48] This was used to allow the dipolar field of the nuclei to reach the coil and give signal which was not present in my cell design.

Tests were conducted concerning how much the B_1 field/signal decreased as different components were added. To obtain a high signal intensity, $LiCoO_2$ was used as the active cathodic material which we hope to observe. The shift range of Li in the static $LiCoO_2$ cathode is between approximately -200 and 200 ppm which is much smaller than in $Li(Ni_{1/3}Mn_{1/3}Co_{1/3})O_2$ resulting in a more intense resonance. The signal at ~250 ppm is attributed to Li metal which experiences a Knight shift (see Figure 4.6).

It was seen that the lithium metal was the component which decreased the signal the most from the base case (and this when separated from the active material by 2 separators (approximately 50 μm)). The 90° pulse length was calibrated for ^{7}Li using pristine $LiCoO_2$. Because the B_1 field is reduced due to the presence of conductive components, more signal could be obtained if each pulse was set to the 90 degree length for each environment.

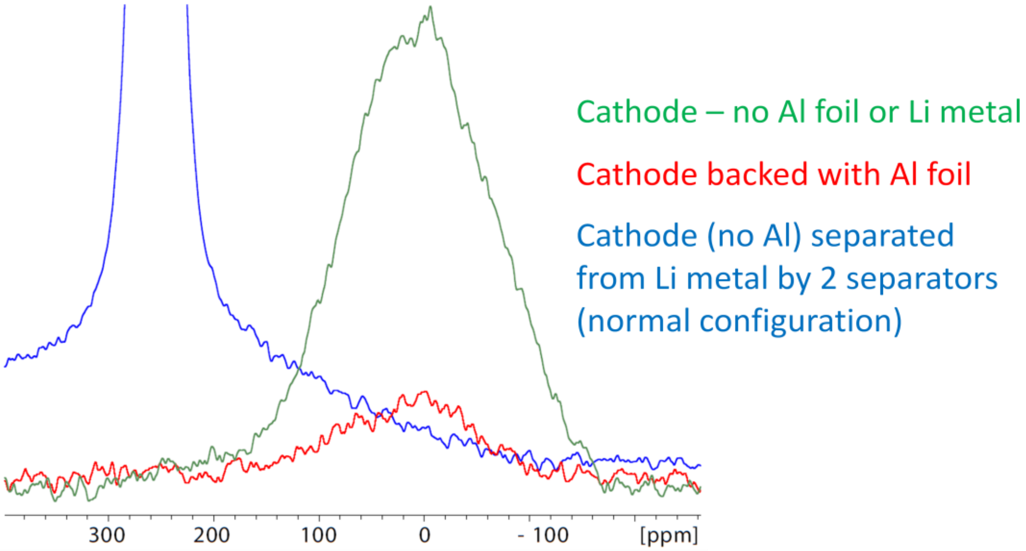

Figure 4.6 Decrease in signal intensity of active material (-200 to 200 ppm) using a solenoid coil with the Swagelok cell and adding different components.

After obtaining parameters from our system, members of Bruce Balcom's University of New Brunswick research group calculated relative field intensities throughout our system in the case of an RF field at 116.6 MHz which corresponds to a 7T field. The results they obtained, shown below, show a far more significant amount of field penetration into the cathode material in the case of a field applied in the plane of the cell. This can be done by using a saddle coil.

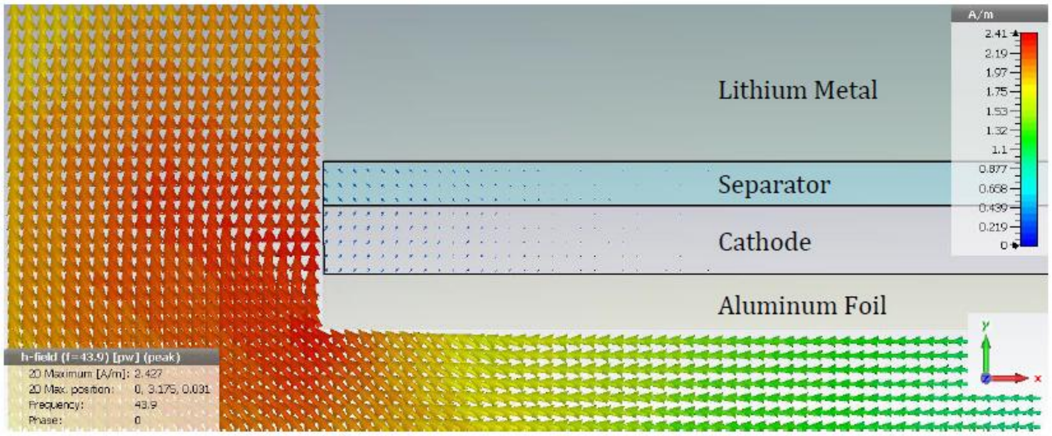

Figure 4.7 RF field intensity of a field applied perpendicular to the cell.

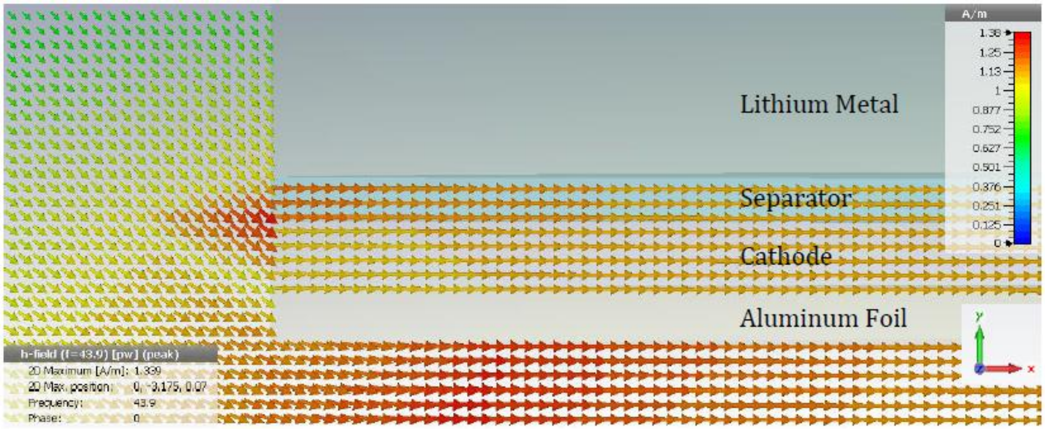

Figure 4.8 RF field intensity of a field applied in the plane of the cell.

Thus, a saddle coil was made which would direct the B_1 field in the plane of the cell. It has four 7 mm by 11 mm turns (two on each side of the cell) of magnet wire which is ~1 mm in diameter. It showed significant improvement in the signal obtained from the fully assembled cell. In fact, the signal obtained for the fully assembled cell was approximately half that of the bare cathode (see Figure 4.9). Like the solenoid coil experiments, the pulse strength and length used was the same as for a 90 degree pulse for

$LiCoO_2$ and thus the signal to noise could likely be improved slightly by recalibration for each experiment.

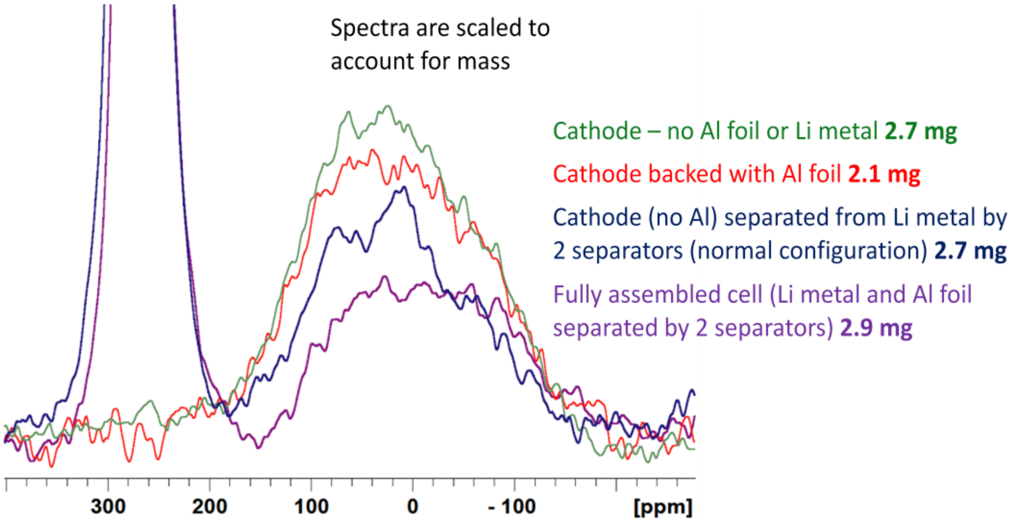

Figure 4.9 Signal intensity achieved from the active material in differing environments to while using the saddle coil with the Swagelok cell.

This lead to the ability to conduct a more feasible *in-situ* cycling experiment with this cell. The magnet used had a field strength of 7.05T corresponding to a B_1 frequency of 166.7 MHz for ^7Li. The results match those obtained by Shimoda et al. who used a plastic bag cell.[49]

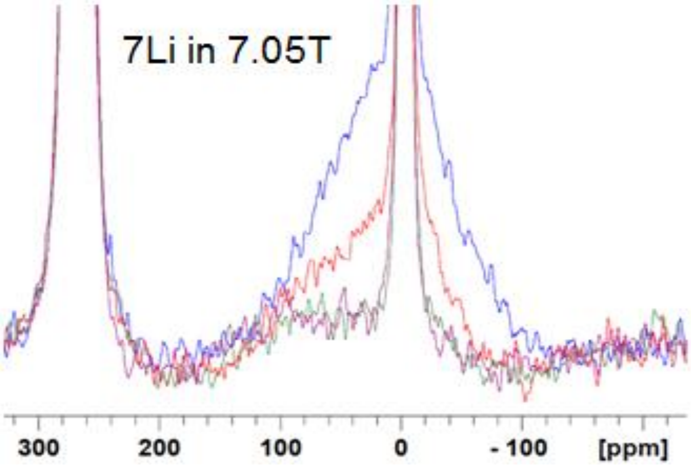

Figure 4.10 Signal obtained from 3.8 mg of $LiCoO_2$ undergoing electrochemical charging in the Swagelok cell using a saddle coil.

4.5 NMR Hardware

Initially, it was decided to modify a training probe to be used for *in-situ* cell use. The only magnets available at this time were narrow-bored and thus the volume available for the cell and RF circuit were restricted. The training probe could tune and match to 85 MHz with a 1 μH coil (which was thought to be adequate to accommodate any cell geometry). After testing, the range of the variable capacitors available was determined to be ~2-10 pF. This was too large of a capacitance to achieve the desired frequencies with the 1 μH coil in a series-parallel circuit depicted below. This circuit was chosen because of its common use, previously solved matching equation and it was the current setup in the training probe.[50]

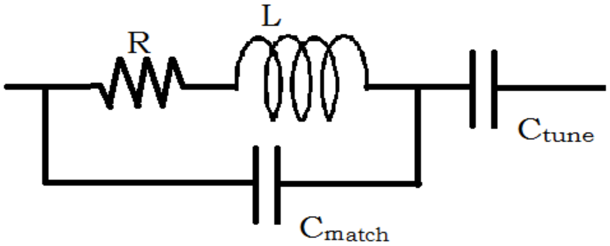

Figure 4.11 Series-parallel tank circuit used in initial NMR probe.

After reading of difficulties experienced by Rathke et al. with variable capacitors, and their higher cost, chip capacitors were purchased which could be placed in series with each capacitor to decrease the capacitance and raise the resonant frequency of the circuit.[45] Solderless arrays for the chip capacitors were built which allowed the quick addition of the desired capacitance in series. These were incorporated in the circuit shown below.

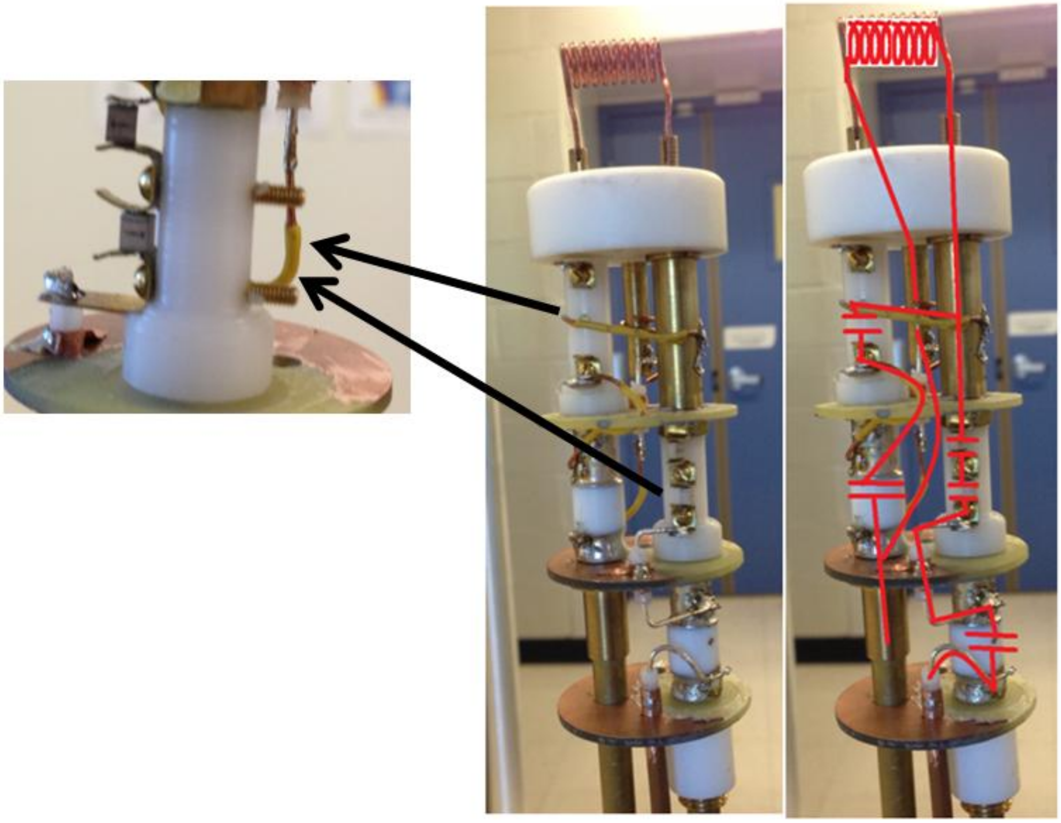

Figure 4.12 The original probe circuit design and the series chip capacitor arrays.

In practice, however, it was very difficult to reach the frequency required. This was found to be due to added capacitance from the aluminum sheath, the copper plating on the platforms (which was scraped off) and the tabs which held the chip capacitors (which were shortened) and potentially the coaxial cable leading to the circuit. This modification raised the matchable range, though not to the desired frequency.

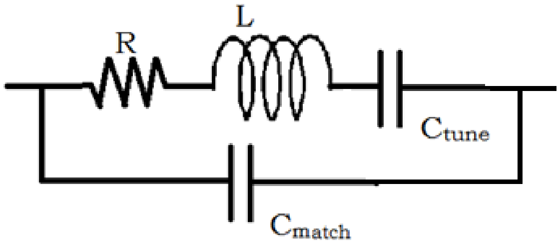

Figure 4.13 A parallel-series tank circuit.

After this realization, a parallel-series circuit (depicted above) was tried. Though more difficult to solve for the matching conditions, upon trial and error it was found that the desired frequencies could easily be reached with just the variable capacitors available; far more than in the series-parallel setup and enough so that the stray capacitances are small or negligible. However, the matching range provided by the 2 to 10 pF is impractically small and likely a larger variable capacitor would be required to allow the circuit to be useable. The acquisition of a wide-bore probe meant that further modification of the training probe was likely not required.

Additionally, a low-pass filter is required to prevent stray electromagnetic noise from being picked up and detected by the NMR circuit. The filter currently used is fairly simple and consists of four inductors (approximately 4 μH and one for each electrochem cable) and two 33 pF RF capacitor joining the two electrochem cables. When used, this filter causes approximately 30 dB of attenuation at 116.7 MHz and gives a spectrum with a S/N ratio the same (within experimental error) as the case with no cables attached (shown below).

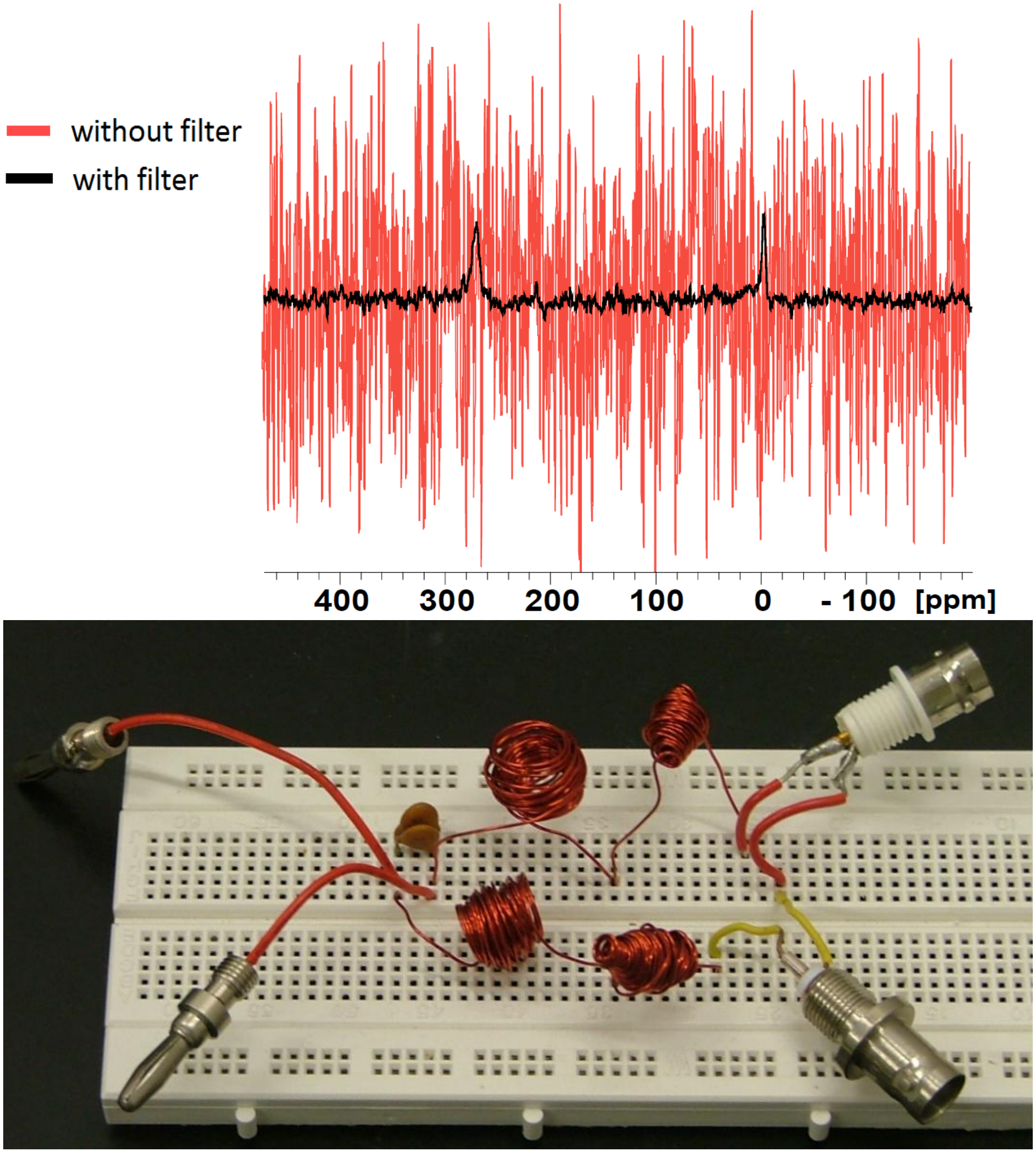

Figure 4.14 (Above) 4 scans of the in-situ cell with and without the filter and (below) a picture of the filter with (from left to right) banana plugs, capacitors, inductors, BNC connectors.

However, care must be taken that the wires between the filter and the probe are placed within the magnet and should have Al foil over the wires and the bore to keep noise from entering beyond the filter.

4.6 Future Work Toward *In-situ* NMR

The *in-situ* cell can still be improved. Firstly, the limits of the active material loading have not been tested and could give more signal. Secondly, for the saddle coil design, there is likely a limit for the Q value of the circuit depending on the capacitance of the probe which currently is a Bruker wide bore probe. The higher the inductance of the coil (the more windings) the more magnetic flux is obtained from the nuclei and the more signal. With this limit in mind there is likely an optimal width of the coil. The two competing factors for this are that a wider coil should give a more homogeneous B_1 field through the sample and have more field lines through it. However, the wider the coil, the fewer turns available due to the inductance limit and this would act to decrease the magnetic flux and thus the signal.

For the in-situ cell, several things may be done to obtain more signal and decrease the amount of shift seen due to bulk magnetic susceptibility. One modification, suggested by Dr. Bruce Balcom, to deliver a fairly homogenous field to the cell is to use the current collectors of the battery as an effective coil; sending the RF pulse current through them to develop a B_1 field.[40] This likely has the advantage of delivering a fairly homogenous field in the centre region of the cell (depending on the shape of the current collector), though less so near the edges of the current collectors, which is also the region of the highest flux density once the nuclei begin to precess (see Figure 4.15 below).

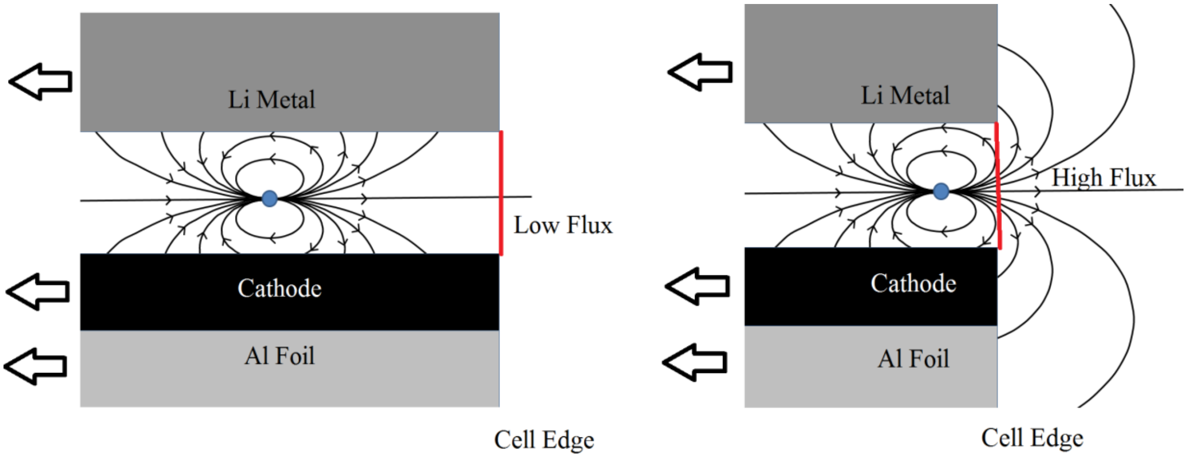

Figure 4.15 The difference in the amount of flux obtained from nuclei near the centre of the cell compared to the edge.

This is in contrast to the saddle coil which is in a region of lower flux (relatively distant from the current collectors) but can have multiple turns, potentially increasing the overall voltage obtained from the sample. It would also give a different amount of field homogeneity in the region of interest, though whether this is higher or lower than the current collector design depends upon the design of the coil and the cell. The author is not certain, at present, which design could obtain the most signal.

In its current form, the in-situ cell would not be amenable to a B_1 generated by current through the collectors as the current would be delivered from the centre of a circular disk, would travel out radially and the B_1 field would be very inhomogeneous.

To use the current collector design well, a new rectangular cell should be built, giving a uniform current density. To obtain the most signal, the edge length should be maximized (Figure 4.15 above). A long skinny cell would work or, because the precessing magnetic field strength decreases rapidly with distance from the cell, multiple long strips could be used in close proximity to occupy as much of the homogeneous B_0 region as possible.

The practicality is that this design may be difficult to manufacture. It would require a rectangular O-ring to make a seal, a way to allow outside electrical access to the current collectors and a way to compress the cells. Though all of this is possible; it would simply need more time to build and use than the Swagelok design.

Assuming that this was made, a setup like that depicted below would allow both radio frequency and direct current through the cell's current collectors while the voltage of the cell and DC current is measured. This setup would block RF noise from affecting the DC measurements (inductors) and would not allow the DC voltage to affect the NMR spectra (blocking capacitors). To the author's knowledge, simultaneous electrochemical measurements and NMR FID acquisition have never been conducted in a cell using a current collector for RF application.

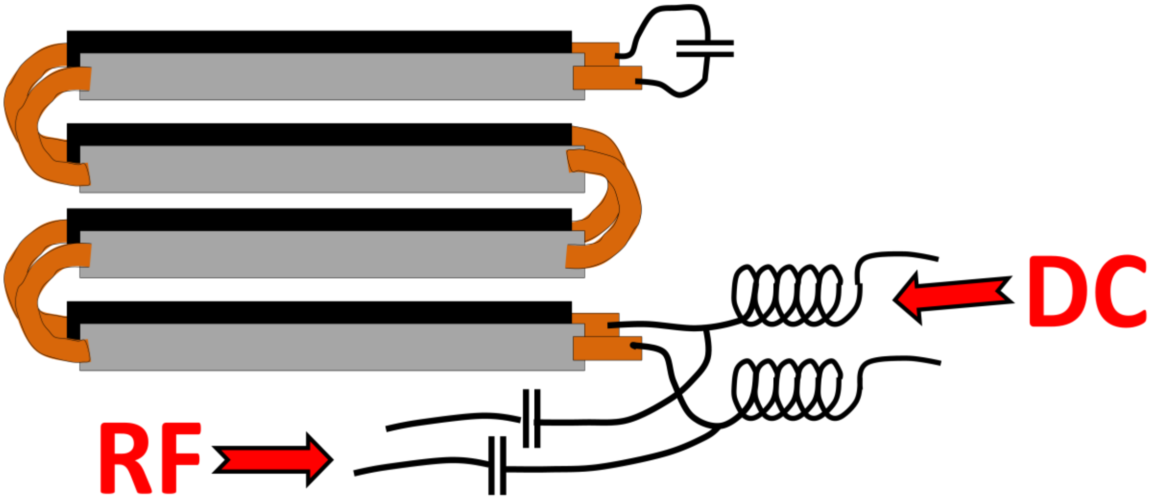

Figure 4.16 A cell design which uses the current collectors as part of the RF circuit (an effective coil). Capacitors block DC from adding an offset during acquisition and carry the RF between anode and cathode. The inductors stop RF pulses being recorded by the electrochemical equipment.

Again, it may be possible to gain more flux from the cell by multiple turns of a saddle coil. Modelling of the flux from the sample should be quite feasible and able to predict which would yield more signal. Additionally, the narrower the cathodes, the less broadening should be observed due to bulk magnetic susceptibility.[30] The sample could be tilted to the magic angle to reduce this as much as possible.

Using these techniques, the signal from the current cell would certainly be increased and may facilitate the acquisition of signals of metastable phases which may appear under high stress cycling.

Chapter 5: Future Work

From the conducted experiments on NMC, we have gained information about the lack of full cation ordering within NMC, the presence of a Ni band allowing good electrical conductivity and the knowledge that Li preferentially leaves sites nearest Mn^{4+}.

This knowledge of the structure of the material may be useful for computational assessments of the material; incorporating it to accurately build a representative structure. This would be done with the end goal of calculating the energy of this phase as compared to the material after a phase transition; understanding why this structure retains its O3 style stacking structure longer than $LiCoO_2$. Once this is known, it may be possible to determine the stoichiometries which would allow the most reversible extraction and thus have the highest energy densities.

Another thing which could be done is to investigate by experimentation whether addition of Mn and Ni (increasing y) would allow more Li to be extracted reversibly. The limit of reversible cycling region is more correlated with the onset of oxygen loss than with an O3 to O2 or O1 change (oxygen position change).[16] Thus, determining the onset of oxygen loss for the $Li(Ni_yMn_yCo_{1-2y})O_2$ class of materials would be interesting to see if increasing Ni^{2+} content is coorelated with a longer extraction profile and may lead to batteries with a higher reversible capacity. This is in addition, of course, to XRD verification and simple long term charging experiments to determine capacity retention.

An additional experiment which would shed more light on the assignments of peaks would be to vary the stoichiometry of NMC according to $Li(Ni_yMn_yCo_{1-2y})O_2$ which would maintain the oxidation states (and thus the shifts) of each of the ions. By the high S/N of ^{7}Li MAS NMR, we can observe slight changes in the peak intensities and thus determine qualitatively how much Co is in each of the sites. For instance, whether the 70 ppm peak increases or decreases in intensity with y should tell which assignment (6 immediate Co neighbours or 4 $(Mn^{4+})^{2nd}$ and 1 $(Mn^{4+})^{1st}$) is correct.

In our investigations of $Li(Li_{0.2}Mn_{0.54}Co_{0.13}Ni_{0.13})O_2$, we determined that the transition metals become disordered as Li is withdrawn from the layer and regain that order when Li is reinserted. It was also seen that after two cycles, the material gains intensities at frequencies near 1000 ppm which is tentatively attributed to Li near Mn in the Li layer and that if discharged further, this intensity is increased.

One experiment which would be of interest would be to vary the length of the plateau to determine the impact of this on capacity as well as the spinel formation and capacity retention. There should be an optimal value of the plateau which would leave many transition metal layer Li sites free but would also allow enough Mn reduction to reinsert all of the Li. This should allow the best performance of the cathode in the reversible cycling domain.

Determining the effects of each transition metal on cycling parameters would likely lead to improvement of this material. In studies by Manthiram et al., the fairly similar materials $Li(Li_{0.2}Mn_{0.6}Ni_{0.2})O_2$ and $Li(Li_{0.2}Mn_{0.54}Ni_{0.13}Co_{0.13})O_2$ had first discharge capacities of approximately 200 mAh/g and 250 mAh/g respectively.[24] If this change in transition metal content gives 25% more capacity, then fine tuning of the transition metal (and Li) content may yield still better capacities. Additionally, each of these materials may show different electrical and ionic impedance, capacity retention and optimal upper and lower cutoff voltages which may be better than the material investigated here.

Additionally, these cells have always shown higher impedance in our studies than their NMC counterparts. They required a C/40 current whereas NMC cells could be run at C/10 (and at least C/3 in the Swagelok cell) without significant overpotential. Thus, one experiment of interest is electrochemical impedance spectroscopy (EIS) which can determine each component's contribution to the overall internal resistance (ion motion in the electrolyte, ion motion in the cathode and electronic motion in the carbon contacts).[51] This, coupled with SEM images of the cathode may yield some clues as to why these cathodes have been giving worse rate performance such as whether densification of the material leads to loss of contact with the carbon electrical conductor.

In the work on the in-situ cell, a cell allowing high compression and rates of cycling was made using a saddle coil to avoid shielding and obtain more signal. This cell may very well allow battery materials to be investigated while subjected to high rates of cycling.

There are, however, additional things which could be attempted to improve this further. If a cell with higher edge length was constructed, there should be a higher amount of signal available due to the increased amount of flux which can escape the edges of the cell. Another modification, suggested by Dr. Bruce Balcom, which could be considered is the application of RF current through the current collectors of the cell.[40] This design would create an effective coil immediately at the edge of the cell and increase the flux obtained though probably limiting the "turns" of the coil to 1. This has not, to the author's knowledge, been implemented before with simultaneous electrical measurements and this could be done as outlined in Chapter 4.

This would allow the investigation of rate-dependent effects which may impact various parts of the cell in high-stress applications such as those experienced in electric vehicles.

Sources

1. Blasing, T. J.
Recent Greenhouse Gas Concentrations. http://cdiac.ornl.gov/pns/current_ghg.html.
2. Canada, N. R. Transportation. http://www.nrcan.gc.ca/energy/efficiency.
3. Tesla Motors, L. Efficiency. http://www.teslamotors.com/goelectric/efficiency.
4. Tarascon, J. M., Issues and Challenges Facing Rechargeable Lithium Ion Batteries. *Nature* **2001,** *414*, 359-367.
5. Goodenough, J. B., Challenges for Rechargeable Li Batteries. *Chemistry of Materials* **2010,** *22*, 587-603.
6. Fultz, B., Howe, J., *Transmission Electron Microscopy and Diffractometry of Materials*. Springer Science and Business Media: 2012.
7. Smiley, D., Davis, L., Goward, G., An Improved Understanding of Li^+ Hopping Pathways and Rates in $Li_3Fe_2(PO_4)_3$ Using Selective Inversion ^{6}Li NMR Spectroscopy. *Journal of Physical Chemistry C* **2013,** *117* (46), 24181-24188.
8. Grey, C. P., NMR Studies of Cathode Materials for Lithium-Ion Rechargeable Batteries. *Chemical Review Papers* **2004,** *104*, 4493-4512.
9. Nagaura, T., Tozawa, K., Lithium Ion Rechargeable Battery. *Prog. Batteries Solar Cells* **1990,** *9*, 209-217.
10. Dahn, J. R., Electrochemical and In Situ X-Ray Diffraction Studies of Lithium Intercalation in LixCo02 *Journal of the Electrochemical Society* **1992,** *139*, 2091.
11. Manthiram, A., Materials Aspects: An Overview. In *Lithium Batteries: Science and Technology* Kluwer Academic Publishers: 2004.
12. Ohzuku, T., Novel Lithium Insertion Material of $LiCo_{1/3}Ni_{1/3}Mn_{1/3}O_2$ for Lithium Ion Batteries. *Journal of Power Sources* **2003,** *171*.
13. Cahill, L. S.; Yin, S. C.; Samoson, A.; Heinmaa, I.; Nazar, L. F.; Goward, G. R., Li-6 NMR studies of cation disorder and transition metal ordering in Li[Ni1/3Mn1/3Co1/3]O-2 using ultrafast magic angle spinning. *Chemistry of Materials* **2005,** *17* (26), 6560-6566.
14. Hwang, B. J.; Tsai, Y. W.; Carlier, D.; Ceder, G., A Combined Computational/Experimental Study on LiNi1/3Co1/3Mn1/3O2. *Chemistry of Materials* **2003,** *15* (19), 3676-3682.
15. Ellis, B., Lee, K. T., Nazar, L., Positive Electrode Materials for Li-Ion and Li-Batteries. *Chem. Mater.* **2010,** *22*, 691-714.
16. Manthiram, A., Role of Chemical and Structural Stabilities on the Electrochemical Properties of Layered $LiNi_{1/3}Mn_{1/3}Co_{1/3}O_2$ Cathodes. *Journal of the Electrochemical Society* **2005,** *152* (9), A1714-1718.
17. Jouanneau, S. D., J. R. , Synthesis, Characterization, and Electrochemical Behaviour of Improved $Li(Ni_xCo_{1-2x}Mn_x)O_2$ ($0.1 < x < 0.5$). *Journal of the Electrochemical Society* **2003,** *150*, A1637-A1642.
18. Whittingham, S., Comparative Study of the Capacity and Rate Capability of $LiNi_yMn_yCo_{1-2y}O_2$. *Journal of the Electrochemical Society* **2011,** *158* (5), A516-A522.
19. Menetrier, M., Saadoune, I., Levasseur, S., Delmas, C. , The insulator–metal transition upon lithium deintercalation from LiCoO2: electronic properties and 7Li NMR study. *J. Mater. Chem.* **1999,** *9*, 1135-1140.

20. Ben Kamel, K., Local structure and electrochemistry of $LiNi_yMn_yCo_{1-2y}O_2$ electrode materials for Li-ion batteries. *Ionics* **2008,** *14*, 89-97.
21. Zeng, D., . Cabana, J., Breger, J., Yoon, W., Grey, C., Cation Ordering in Li[NixMnxCo(1–2x)]O2-Layered Cathode Materials: A Nuclear Magnetic Resonance (NMR), Pair Distribution Function, X-ray Absorption Spectroscopy, and Electrochemical Study. *Chem. Mater.* **2007,** *19* 6277-6289.
22. Dahn, J. R., Understanding the Anomalous Capacity of $Li/Li(Ni_xLi_{1/3-2x/3)}Mn_{(2/3-x/3)})O_2$ Cells Using In Situ X-Ray Diffraction and Electrochemical Studies. *Journal of the Electrochemical Society* **2002,** *149*, A815-A822.
23. Li, Y., Bettge, M., Polzin, B., Zhu, Y., Balasubramanian, M., Abraham, D. P., Understanding Long-Term Cycling Performance of Li1.2Ni0.15Mn0.55Co0.1O2–Graphite Lithium-Ion Cells. *Journal of the Electrochemical Society* **2013,** *160* (5), A3006-A3019.
24. Manthiram, A., Influence of Cationic Substitutions on the Oxygen Loss and Reversible Capacity of Lithium-Rich Layered Oxide Cathodes. *Journal of Physical Chemistry C* **2011,** *115*, 7097-7103.
25. Hideyuki, K., Croguennec, L., Mannessiez, P., Menetrier, M., Weill, F., Bourgeois, L., Duttine, M., Suard, E., Delmas, C., Li1.20Mn0.54Co0.13Ni0.13O2 with Different Particle Sizes as Attractive Positive Electrode Materials for Lithium‑Ion Batteries: Insights into Their Structure. *J. Phys. Chem. C.* **2012,** *116*, 13497-13506.
26. Breger, J., Jiang, M., Dupre, N., Meng, Y., Shao-Horn, Y., Ceder, G., Grey, C., High-resolution X-ray diffraction, DIFFaX, NMR and first principles study of disorder in the Li2MnO3–Li[Ni1/2Mn1/2]O2 solid solution. *J. Solid State Chem.* **2005,** *178*, 2575-2585.
27. Grey, C. P., Local Structure and Cation Ordering in O3 Lithium Nickel Manganese Oxides with Stoichiometry Li(NixLi(1/3-2x/3)Mn(2/3-x/3))O2 *Electrochemical and Solid State Letters* **2004,** *7* (7), A167-A171.
28. Ceder, G., Electrochemical Activity of Li in the Transition Metal Sites of O3 $Li(Li_{(1-2x)/3}Mn_{(2-x)/3}Ni_x)O_2$. *Electrochemical and Solid State Letters* **2004,** *7* (9), A290-293.
29. Labs, L. B. N. Nuclear Moments. http://ie.lbl.gov/toipdf/mometbl.pdf.
30. Trease, N. M., Zhou, L., Chang, H. J., Zhu, B. Y., Grey, C. P, In situ NMR of lithium ion batteries: Bulk susceptibility effects and practical considerations. *Solid State Nuclear Magnetic Resonance* **2012,** *42*, 62-70.
31. Stoyanova, R., Correlations between lithium local structure and electrochemistry of layered LiCo(1-2x)Ni(x)Mn(x)O2 oxides: 7Li MAS NMR and EPR studies. *Phys Chem Chem Phys* **2014,** *16* (6), 2499-507.
32. Pell, A. J. In *Introduction to Paramagnetic NMR*, University of Cambridge, University of Cambridge, 2014.
33. Duer, M. J., Solid State NMR Spectroscopy: Principles and Applications. Blackwell Science Ltd. : Cambridge, 2002.
34. Yabuuchi, N.; Ohzuku, T., Novel lithium insertion material of LiCo1/3Ni1/3Mn1/3O2 for advanced lithium-ion batteries. *Journal of Power Sources* **2003,** *119*, 171-174.
35. Whitfield, P. S., Davidson, I. J., Cranswick, L. M. D., Swainson, I. P., Stephens, P. W., Investigation of possible superstructure and cation disorder in the lithium battery cathode material LiMn1/3Ni1/3Co1/3O2 using neutron and anomalous dispersion powder diffraction. *Solid State Ionics* **2005,** *176*, 463-471.

36. Yoon, W. S., Balasubramanian, M., Chung, K. Y., Yang, X. Q., McBreen, J., Grey, C. P., Fischer, D. A., Investigation of the Charge Compensation Mechanism on the Electrochemically Li-Ion Deintercalated Li1-xCo1/3Ni1/3Mn1/3O2 Electrode System by Combination of Soft and Hard X-ray Absorption Spectroscopy. *J. Am. Chem. Soc.* **2005,** *127*, 17479-17487.

37. Reale, P., Privitera, D., Panero, S., Scrosati, B., An investigation on the effect of Li+/Ni2+ cation mixing on electrochemical performances and analysis of the electron conductivity properties of LiCo0.33Mn0.33Ni0.33O2. *Solid State Ionics* **2007,** *178*, 1390-1397.

38. Hung, I., Gan, Z. H., , On the magic-angle turning and phase-adjusted spinning sidebands experiments. *J. Magn. Res.* **2010,** *204*, 150-154.

39. Tran, N., Croguennec, L., Menetrier, M., Weill, F., Biensan, Ph., Jordy, C., Delmas, C., Mechanisms Associated with the "Plateau" Observed at High Voltage for the Overlithiated $Li_{1.12}(Ni_{0.425}Mn_{0.425}Co_{0.15})_{0.88}O_2$ System. *Chem. Mater.* **2008,** *20*, 4815-4825.

40. Zhang, Z. M., J., Wu, J., Wang, H., Promislow, K., Balcom, B., Magnetic resonance imaging of water content across the Nafion membrane in an operational PEM fuel cell. *Journal of Magnetic Resonance* **2008,** *193*, 259-266.

41. Zhou, L., Leskes, M., Ilott, A., Trease, N. M., Grey, C. P., Paramagnetic electrodes and bulk magnetic susceptibility effects in the in situ NMR studies of batteries: Application to $Li_{1.08}Mn_{1.92}O_4$ spinels. *Journal of Magnetic Resonance* **2013,** *234*, 44-57.

42. Nazri, G.-A., Pistoia, G., *Lithium Batteries: Science and Technology*. 2003.

43. Zheng, J., Gu, M., Xiao, J., Zuo, P., Wang, C., Zhang, J-G., Corrosion/Fragmentation of Layered Composite Cathode and Related Capacity/Voltage Fading during Cycling Process. *Nano. Lett.* **2013,** *13*, 3824-3830.

44. Grey, C. P., Real-Time NMR Investigations of Structural Changes in Silicon Electrodes for Lithium-Ion Batteries. *J. Am. Chem. Soc.* **2009,** *131*, 9239-9249.

45. Rathke, J., Klinger, R., Gerald, R., Kramarz, K., Woelk, K., Toroids in NMR Spectroscopy. *Prog. Nucl. Magn. Reson. Spectrosc.* **1996,** *30*, 209-253.

46. Gerald, R. E., Sandi, G., Johnson, C. S., Scanlon, L. G., Rathke, J. W., ^7Li NMR study of intercalated lithium in curved carbon lattices. *Journal of Power Sources* **1999,** *89*, 237-243.

47. Chevalier, F., Letellier, M., Morcrette, M., Tarascon, J.-M., Frackowiak, E., Rouzaud, J.-N., Beguin, F., In-Situ ^7Li-Nuclear Magnetic Resonance Observations of Reversible Lithium Insertion into Disordered Carbons. *Electrochemical and Solid State Letters* **2003,** *6*, A225-A228.

48. Poli, F., Kshetrimayum, J., Monconduit, L., Letellier, M., New cell design for in-situ NMR studies of lithium ion batteries. *Electrochemistry Communications* **2011,** *13*, 1293-1295.

49. Shimoda, K., Murakami, M., Takamatsu, D., Arai, H., Uchimoto, Y., Ogumi, Z., In situ NMR observation of the lithium extraction/insertion from $LiCoO_2$ cathode. *Electrochemica Acta* **2013,** *108*, 343-349.

50. (a) Jiang, Y., J., A Simple Method for Measuring the Q Value of an NMR Sample Coil. *Journal of Magnetic Resonance* **2000,** *142*, 386-388; (b) Fukushima, E., Roeder, S., *Experimental Pulse NMR*. Addison-Wesley Publishing Company: New York, 1981.

51. Van Bommel, A., Divigalpitiya, R., Effect of Calendaring LiFePO4 Electrodes. *Journal of the Electrochemical Society* **2012,** *159* (11), A1791-A1795.